Lecture 5 — Scattering geometries.

1 Introduction

In this section, we will employ what we learned about the interaction between radiation and matter, as well as the methods of production of electromagnetic and particle beams, do describe a few "realistic" geometries for single-crystal and powder diffraction experiments. Throughout this discussion, we will assume that the crystals under investigation are "ideal" — in particular, that they are free from defects and have perfect translational invariance (i.e., they are of infinite extent). At the same time, we will assume that the interaction between the beam and the crystal is "weak", so that we can ignore multiple-scattering effect. This approximation is known as the **kinematic approximation**. We will relax the kinematic approximation at the end of this lecture, where we will discuss (somewhat qualitatively) the so-called **dynamical diffraction**. The next lecture will be devoted to the discussion of crystal defects, starting from the ones arising from the finite size of real crystals.

2 Cross section for a "small" perfect single crystal

Our goal in this section is to calculate the scattering cross section from a "small" single crystal. We will employ a series of key assumptions, some of which will be later relaxed.

- The crystal is large enough that we can effectively sum over an "infinite" number of unit cells. This seems a paradoxical assumption, especially for what we call a "small" single crystal, but it turns out that crystal size effects are not important even for a crystal as small as 10 μm. In the next lecture, we will relax this approximation and calculate the cross section including finite-size effects.

- The crystal is small compared to the geometrical distances of the measuring apparatus. This means we can still use the "far-field" approximation we have employed throughout the derivation of the atomic scattering cross sections. As we shall see at the end of this lecture, relaxing this approximation is essential to discuss dynamical diffraction effects.

- We can neglect multiple scattering — in other words, we will consider the scattered wave as freely propagating outside the sample and towards the detector. This is a severe approximation, which in most cases is far from the truth. One first, simple correction to this approximation is made by considering **attenuation effects**, both of the incident beam and of the scattered beam. In other words, we could say that some of the incident/scattered

beam is simply lost because it is absorbed by the sample itself, or it is scattered in a direction other than that of the incident or main scattered beams. However, this correction is in general not sufficient for large crystals, this simple "**kinematic**" theory of crystal scattering becomes inadequate and one has to tackle the problem in the framework of the so-called "**dynamical theory**" of crystal scattering. The most general manifestation of the inadequacy of kinematic theory is the fact is not energy-conserving. We will discuss these issues later in the course.

- We consider the crystal to be "perfect", most notably perfectly periodic. This is, of course, never true, most notably due to atomic vibrations. We will see shortly how to take atomic vibrations into account in calculating the cross sections. Other types of defects (e.g., point defects, dislocations etc.) will be discussed in the next lecture.

For the sake of argument, we will treat the case of X-rays, although, as we shall see, the other cases (neutrons, electron beams) yield very similar results. Using the far-field approximation, we can develop exactly the same argument we used to calculate the form factors, but, this time, we extend the volume integral to the *whole crystal*. Following the same procedure explained in the previous lecture, the scattering density becomes:

$$\boxed{A(\mathbf{q}) = r_0 \int_{Crystal} d\mathbf{R} f(\mathbf{R}) e^{-i\mathbf{q}\cdot\mathbf{R}} \left[\boldsymbol{\epsilon}\cdot\boldsymbol{\epsilon}'\right]} \tag{1}$$

We can exploit the fact that the charge density is periodic, so that, if $\mathbf{R}_i$ is a lattice translation and $\mathbf{r}$ is restricted to the unit cell containing the origin:

$$f(\mathbf{R}) = f(\mathbf{R}_i + \mathbf{r}) = f(\mathbf{r}) \tag{2}$$

whence the scattering amplitude becomes

$$\begin{aligned} A(\mathbf{q}) &= r_0 \sum_i \int_{Unit\,Cell} d\mathbf{r} f(\mathbf{r}) e^{-i\mathbf{q}\cdot(\mathbf{R}_i+\mathbf{r})} \left[\boldsymbol{\epsilon}\cdot\boldsymbol{\epsilon}'\right] \\ &= r_0 \sum_i e^{-i\mathbf{q}\cdot\mathbf{R}_i} \int_{Unit\,Cell} d\mathbf{r} f(\mathbf{r}) e^{-i\mathbf{q}\cdot\mathbf{r}} \left[\boldsymbol{\epsilon}\cdot\boldsymbol{\epsilon}'\right] \end{aligned} \tag{3}$$

where the summation runs over all the unit cells in the crystal. The expression

$$\boxed{F(\mathbf{q}) = r_0 \int_{Unit\,Cell} d\mathbf{r} f(\mathbf{r}) e^{-i\mathbf{q}\cdot\mathbf{r}}} \tag{4}$$

is known as the **structure factor**.

The structure factor is proportional to the Fourier transform of the charge density (or, more in general, scattering density) integrated over the unit cell.

If the electron density $f(\mathbf{r})$ is a superposition of atomic-like electron densities, it is easy to show that $F(\mathbf{q})$ can be written as

$$\boxed{F(\mathbf{q}) = r_0 \sum_n f_n(\mathbf{q}) e^{-i\mathbf{q}\cdot\mathbf{r}_n}} \tag{5}$$

where the sum runs over all the atoms in the unit cell and $f_n(\mathbf{q})$ are the form factors of each species and $\mathbf{r}_n$ are their positions within the unit cell.

We can now calculate the cross section:

$$\frac{d\sigma}{d\Omega} = A(\mathbf{q})A^*(\mathbf{q}) = \left(\sum_j \sum_i e^{-i\mathbf{q}\cdot(\mathbf{R}_i - \mathbf{R}_j)} \right) |F(\mathbf{q})|^2 \left[\boldsymbol{\epsilon} \cdot \boldsymbol{\epsilon}' \right]^2 \tag{6}$$

We now introduce the fact that the double summation in parentheses can be consider as running over an infinite lattice. Consequently, all the summations over i labelled by $\mathbf{r}_j$ are the same (they only differ by a shift in origin), and the summation over j can be replaced by multiplication by N_c — the number of unit cells in the crystal ($\rightarrow \infty$).

As we have already remarked, the remaining single summation is only non-zero when $\mathbf{q}$ is a RL vector. If $\mathbf{q}$ is restricted to the first Brillouin zone, we can write:

$$\delta(\mathbf{q}) = \frac{1}{(2\pi)^3} \int d\mathbf{x} e^{-i\mathbf{q}\cdot\mathbf{x}} \simeq \frac{v_0}{(2\pi)^3} \sum_i e^{-i\mathbf{q}\cdot\mathbf{R}_i} \tag{7}$$

where v_0 is the unit cell volume. For an unrestricted $\mathbf{q}$, the same expression holds with the left-hand member replaced by a sum of delta functions centred at all reciprocal lattice nodes, indicated with $\boldsymbol{\tau}$ in the remainder. With this, we can write the final expression for the cross section:

$$\frac{d\sigma}{d\Omega} = N_c \frac{(2\pi)^3}{v_0} \sum_{\boldsymbol{\tau}} \delta(\mathbf{q} - \boldsymbol{\tau}) |F(\boldsymbol{\tau})|^2 \left[\boldsymbol{\epsilon} \cdot \boldsymbol{\epsilon}'\right]^2 \tag{8}$$

As in the case of the scattering from a single electron or atom, the term $\left[\boldsymbol{\epsilon} \cdot \boldsymbol{\epsilon}'\right]^2$ needs to be averaged over all this incident and scattered polarisations, yielding a **polarisation factor** $\mathcal{P}(\gamma)$, which depends on the experimental setting. For example, for an unpolarised incident beam and no polarisation analysis:

$$\boxed{\mathcal{P}(\gamma) = \left[\frac{1 + \cos^2 \gamma}{2}\right] \quad \textbf{unpolarised beam}} \tag{9}$$

The final general expression for the average cross section is:

$$\boxed{\frac{d\sigma}{d\Omega} = N_c \frac{(2\pi)^3}{v_0} \sum_{\boldsymbol{\tau}} \delta(\mathbf{q} - \boldsymbol{\tau}) |F(\boldsymbol{\tau})|^2 \mathcal{P}(\gamma)} \tag{10}$$

Let's recap the key points to remember:

- **The cross section is proportional to the number of unit cells in the crystal. The bigger the crystal, the more photons or particles will be scattered. We can clearly see that this result *must* involve an approximation: the scattered intensity must reach a limit when all the particles in the beam are scattered.**
- **The cross section is proportional to the squared modulus of the structure factor (no surprises here — you should have learned this last year).**
- **Scattering only occurs at the nodes of the RL. For a perfect, infinite crystal, this is in the form of delta functions.**
- **The cross section contains the unit-cell volume in the denominator. This is necessary for dimensional reasons, but it could perhaps cause surprise. After all, we could arbitrarily decide to *double* the size of the unit cell by introducing a "basis". The answer is, naturally, that the $|F(\boldsymbol{\tau})|^2$ term exactly compensates for this.**

3 The effect of atomic vibrations — the Debye-Waller factor

3.1 D-W factors — qualitative discussion

Up to this point, we have explicitly assumed perfect periodicity — in other words, that the electron densities of all the unit cells are identical, or, for atomic-like electron densities, that the atoms are in identical positions in all unit cells. This is, of course, never the case. Atoms are always displaced away from their "ideal" positions, primarily due to thermal vibrations, but also due to crystal defects. We now want to examine the effect of these displacements and relax the perfect periodicity condition. Let us re-write the expression of the scattering amplitude (eq. 3), adapted to the atomic case (we omit the polarisation factor $[\boldsymbol{\epsilon} \cdot \boldsymbol{\epsilon}']^2$ for simplicity):

$$A(\mathbf{q}) = r_0 \sum_i e^{-i\mathbf{q}\cdot\mathbf{R}_i} \sum_n f_n(\mathbf{q}) e^{-i\mathbf{q}\cdot(\mathbf{r}_n + \mathbf{u}_{n,i})} \tag{11}$$

where $\mathbf{u}_{n,i}$ is the *displacement vector* characterising the position of the atom with label n in the i^{th} unit cell.

The expression 11 would be appropriate for *static* displacements. However, typical phonon frequencies at room temperature are of the order of a few THz, whereas the typical diffraction experiment last several minutes, so some time averaging is clearly required. Herein lies an important question: what do we need to average — the cross section or the scattering amplitude? In the former case, each scattering event would see an instantaneous "frozen snapshot" of the crystal, and the final "pattern" would result from a superposition of these "snapshots — obtained by simply adding up the intensities. In the latter case, the scattering density (electron density, nuclear density) around each site will be "smeared out", pretty much as we have seen to be the case for the form factors. We give here a "hand-waving" argument of why the latter strategy is the appropriate one, deferring to more advanced courses the full derivation, which involves the calculation of the full dynamical structure factor. In essence, Bragg scattering is an elastic process, so the energy transfer is exactly defined (zero, in this case). Since energy and time are conjugated variables, if energy is completely determined then time must be completely undetermined — in other words, Bragg scattering must result from time averaging of the scattering *amplitude*. So, to summarise this discussion

Atomic vibrations "smear out" the scattering density, acting, in a sense as an additional "form factor".

- **The higher the temperature, the more the atoms will vibrate, the more the intensity will decay at high q. This is easily understood by analogy with the form factor $f(\mathrm{q})$: the more the atoms vibrate, the more "spread" out the scatter8ing density will be, the faster the scattering will decay at high q.**
- **The *softer* the spring constants, the more the atoms will vibrate, the more the intensity will decay at high q.**
- **The *lighter* the atoms, the more the atoms will vibrate, the more the intensity will decay at high q.**

3.2 D-W factors — functional form

Being content with this qualitative discussion for the moment, we can re-write eq. 11 as

$$A(\mathbf{q}) = r_0 \sum_i e^{-i\mathbf{q}\cdot\mathbf{R}_i} \sum_n f_n(\mathbf{q}) e^{-i\mathbf{q}\cdot\mathbf{r}_n} \left\langle e^{-i\mathbf{q}\cdot\mathbf{u}_{n,i}} \right\rangle \tag{12}$$

where $\langle\rangle$ indicates time averaging. Needless to say that the expression in $\langle\rangle$ *does not depend on i*, since, once the averaging is performed, the position of the unit cell in the crystal is immaterial (they will all average to identical values). We already see from here that *the effect of thermal vibrations can be incorporated in the structure factor*. To complete our derivation, we need one more step, known as the **Bloch's identity**, which is valid in the harmonic approximation. We will just state the result here:

$$\left\langle e^{-i\mathbf{q}\cdot\mathbf{u}_{n,i}} \right\rangle = e^{\frac{1}{2}\left\langle(-i\mathbf{q}\cdot\mathbf{u}_n)^2\right\rangle} = e^{-\frac{1}{2}\left\langle(\mathbf{q}\cdot\mathbf{u}_n)^2\right\rangle} = e^{-W(\mathbf{q},n)}. \tag{13}$$

W is a positive-definite quantity, known as the **Debye-Waller factor**. It is also a *quadratic function of* $\mathbf{q}$, so its most general expression is

$$W(\mathbf{q},n) = U^{ij}(n) q_i q_j = \mathbf{q}\overline{\overline{\mathbf{U}}}_n\mathbf{q} \tag{14}$$

where $U^{ij}(n)$ is, in general, a *tensor*.

Here, n labels the specific atomic site.

3.2.1 Isotropic case

When all atoms vibrate with the same amplitude in all directions **isotropic case**, $U^{ij}(n)$ is proportional to the unit matrix and

$$\boxed{W(\mathbf{q}, n) = U_n\, q^2} \tag{15}$$

With this, we obtain the **general expression for the X-ray structure factor in the isotropic case**

$$\boxed{F(\mathbf{q}) = r_0 \sum_n f_n(q) e^{-i\mathbf{q}\cdot\mathbf{r}_n} e^{-U_n\, q^2}} \tag{16}$$

A very similar expression is found for the ***coherent*** **neutron factor in the isotropic case**

$$\boxed{F(\mathbf{q}) = \sum_n b_n e^{-i\mathbf{q}\cdot\mathbf{r}_n} e^{-U_n\, q^2}} \tag{17}$$

3.2.2 General (anisotropic) case

A few words here for the general case: **anisotropic vibrations** are actually very common, since atoms tent to vibrate more in the direction *perpendicular* to the bonds connecting them. In the first approximation, the average scattering density can be approximated by a positive-definite *quadratic form*, known as a **thermal ellipsoid**. It is rather intuitive that these thermal ellipsoids **must be constrained by symmetry** — in other words, if the atom is on a mirror plane, one of the principal axes of the ellipsoid must be orthogonal to the plane, etc. When one takes into account he site symmetry, therefore, it transpires that only certain components of $U^{ij}(n)$ are allowed on specific sites, and relations are set between components within each U-tensor and between U-tensors on symmetry-related sites.

3.2.3 Temperature dependence of the Debye-Waller factors

As we have seen in the previous sections, the Debye-Waller factor is related to the amplitude of the vibration and therefore both to the **phonon spectrum** and to the **tremperature**. It can be

shown (see [1] vol 1 p 108-110) that **for an isotropic, monoatomic solid of atomic mass M the expression for W is**:

$$W(q,T) = \frac{\hbar^2 q^2}{4M} \int d\omega \frac{Z(\omega)}{\omega} \coth(\frac{1}{2}\hbar\omega\beta) \tag{18}$$

where $Z(\omega)$ is the **phonon density of states** and $\beta = 1/k_B T$.

Here we report the result for a **single oscillator (Einstein model)**, where $Z(\omega) = \delta(\omega - \omega_E)$:

$$\boxed{W_E(q,T) = \frac{\hbar^2 q^2}{4M\omega_E} \coth(\frac{1}{2}\hbar\omega_E\beta)} \tag{19}$$

In spite of its simplicity, eq. 19 is often employed to fit the temperature dependence of the Debye-Waller factors.

4 Laue and Bragg equations

The δ function in eq. 8 implicitly contains the geometrical conditions for observing scattering from a single crystal, which are traditionally named **Laue equations** [1]:

$$\mathbf{q} = h\mathbf{a}^* + k\mathbf{b}^* + l\mathbf{c}^* \tag{20}$$

$$\begin{aligned} \mathbf{q}\cdot\mathbf{a}_1 &= (\mathbf{k}_f - \mathbf{k}_i)\cdot\mathbf{a}_1 = 2\pi h \\ \mathbf{q}\cdot\mathbf{a}_2 &= (\mathbf{k}_f - \mathbf{k}_i)\cdot\mathbf{a}_2 = 2\pi k \\ \mathbf{q}\cdot\mathbf{a}_3 &= (\mathbf{k}_f - \mathbf{k}_i)\cdot\mathbf{a}_3 = 2\pi l \end{aligned} \tag{21}$$

where h, k and l are the **Miller indices** that we have already encountered.

The Laue equations are nothing but a re-statement of the fact that *q* must be a RL vector

A second important relation can be obtained by considering the *modulus* of the scattering vector, for which, as we have already seen (fig. 1 and eq. 22 are reproduced here for convenience):

[1] Throughout this part of the course, we will employ the convention that $\boldsymbol{q}$ is *the change of wavevector of the particle or photon*, so $\boldsymbol{q} = \boldsymbol{k}_f - \boldsymbol{k}_i$. the convention $\boldsymbol{q} = \boldsymbol{k}_i - \boldsymbol{k}_f$ identifies $\boldsymbol{q}$ with the wavevector *transferred to the crystal*, and is widely employed particularly in the context of inelastic scattering

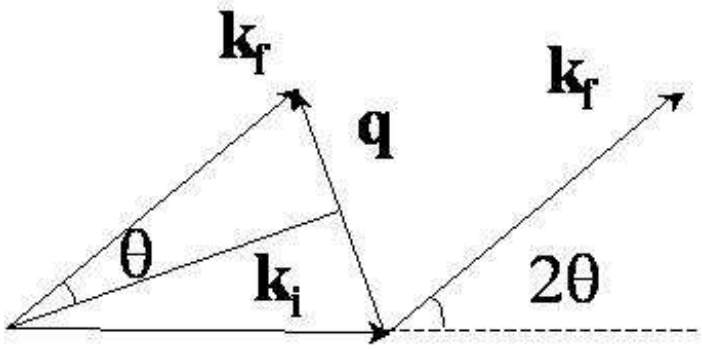

Figure 1: Scattering triangle for elastic scattering.

$$q = |\mathbf{q}| = \frac{4\pi \sin\theta}{\lambda} \tag{22}$$

The quantity

$$\boxed{d = \frac{2\pi}{q}} \tag{23}$$

is known as the **d-spacing**. From eqs. 22 and 23 we obtain the **familiar formulation of Bragg's law**:

$$\boxed{2d \sin\theta = \lambda} \tag{24}$$

As shown in Appendix I, **the d-spacing can be identified with the spacing between families of lattice planes *perpendicular* to a given RL vector**.

5 Geometries for diffraction experiments

In general terms, the experimental apparatus to perform a diffraction experiment on a single crystal or a collection of small crystals (powder diffraction) will consist of

- An **incident beam**, which can be **monochromatic** or **polychromatic**. The **divergence** of the incident beam is of course an important parameter, in that it determines the uncertainty

on the Bragg angle 2θ. Various focussing schemes are possible to increase the flux on the sample or at the detector position whilst limiting the loss of resolution.

- A **sample stage**, which enables the sample to be oriented (typically a simple uniaxial rotator for powder diffraction, a Eulerian cradle or analogous arrangements for single crystal experiments). The sample stage also incorporates the **sample environment** to control a variety of physical (P, T, H...) and/or chemical parameters.

- A **detector**, which includes a detector of photons or particles. Many technologies are available (gas tube, scintillator, CCD, solid-state...), depending on the type of radiation, detector coverage and resolution required. This is normally mounted on a separate arm, enabling the 2θ angular range to be varied. On the detector arm, one often finds other devices, such as as **analyser crystal** and/or **receiving slits** to define the angular divergence of the scattered beam and, in the case of the analyser, to reject parasite radiation due to fluorescence.

In this section, we will focus on two among the most important important geometries for diffraction experiments: the **single-crystal 4-circle diffractometer** and the **Debye-Scherrer powder diffractometer**. Several other geometries are described in Appendix II. In their simplest form, both these geometries employ a **point detector**, with a spatial resolution defined by a set of vertical and horizontal slits. Early diffractometers made extensive use of **photographic film**. Modern single-crystal and powder diffractometers generally employ a **pixillated area detector**. As an introduction to each method, we will describe two important geometrical constructions: the **Ewald construction** (most useful for single-crystal experiments) and the **Debye-Scherrer construction** (for powder diffraction).

5.1 Single-crystal diffraction

5.1.1 The Ewald construction

As we have seen, the scattering cross section for a single crystal is a series of delta functions in reciprocal space, centred at the nodes of the reciprocal lattice. When a single crystal is illuminated with monochromatic radiation, the scattering conditions are satisfied only for particular orientations of the crystal itself — in essence, the specular (mirror-like) reflection from a family of lattice planes must satisfy Bragg law at the given wavelength.

With monochromatic radiation, for a generic crystal orientation, no Bragg scattering will be observed at all.

The German physicist Paul Peter Ewald devised a very useful graphical construction, known as the **Ewald construction**, to establish the orientation of the crystal axes with respect to the

incident beam required to satisfy the scattering conditions. Although largely superseded as a practical calculation device, Ewald construction is of great pedagogical value to illustrate single-crystal scattering (not exclusively with monochromatic radiation), and we will illustrate it here in some detail.

The Ewald construction is made in the following steps (see fig. 2)

1. A **reciprocal lattice plane**, coinciding with the **scattering plane**, is drawn first, in an arbitrary orientation.
2. The **incident beam direction** is then marked with **a line through the origin of the** RL.
3. The **incident wavevector** $\mathbf{k}_i$ is drawn with an **arrow**, with the **point at the origin of the** RL and of **the appropriate length to be at the correct scale** (same conversion, say, between Å^{-1} and cm^{-1}) with respect to the RL.
4. A **circle centred on the *tail* of the arrow**, and **passing through the origin of the** RL is drawn. In a full 3-dimensional construction, the circle would be replaced with a sphere, so they are both known as the **Ewald sphere**.
5. Scattering conditions are met whenever **the Ewald sphere intercepts one of the** RL **nodes**.
6. To set the scattering angle 2θ (also refered to as γ in the remainder), one draws a **second arrow with the same origin and length, making an angle** 2θ **with the first**. This arrow represents the **scattered wavevector** $\mathbf{k}_f$. The scattering vector $\mathbf{q}$ is obviously the **difference vector** $\mathbf{k}_f - \mathbf{k}_i$.
7. To observe the effect of rotating the crystal, one can rotate the whole RL whilst keeping $\mathbf{k}_i$ and $\mathbf{k}_f$ fixed.
8. To represent **crystal rotation** by an angle, say ϕ, one should **draw a second reciprocal lattice** rotated by ϕ with respect to the first. However, the drawing is a lot less cluttered if one **rotates the incident beam** by $-\phi$ instead. This is done in several of the drawings that follow.
9. For wavelength-dispersive techniques, spheres of different radii are drawn to represent the *minimum wavelength* (large sphere) and *maximum wavelength* (small sphere) employed in the experiment.

5.1.2 An application of the Ewald construction: azimuthal scans

We can illustrate the usefulness of the Ewald construction by straightforwardly obtaining a non-trivial result about crystal orientations riving rise to scattering for a certain RL node $\boldsymbol{\tau}$. As we can

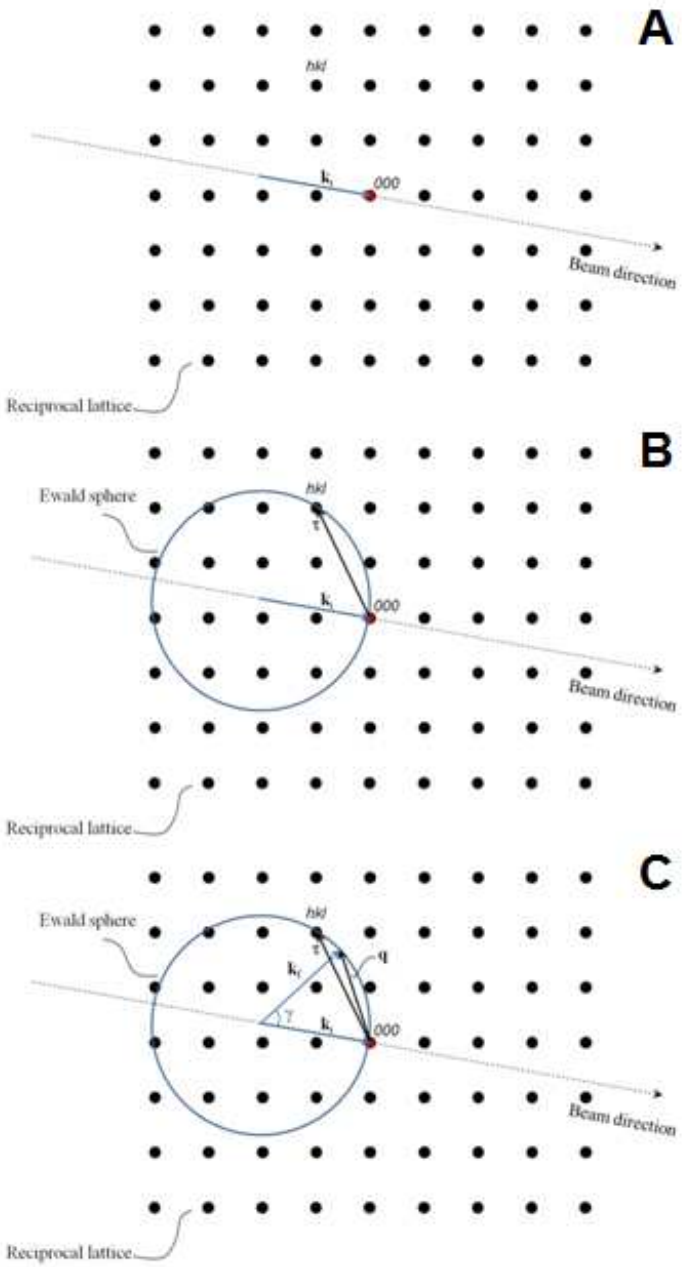

Figure 2: A step-by-step illustration of the Ewald construction.

see from fig. 3, we can rotate the whole Ewald construction around the scattering vector whilst maintaining the scattering conditions. In practical terms, one rotates the *crystal* for a constant beam direction — an operation known as an **azimuthal scan**. The *intensity* of a Bragg reflection does not in general remain constant through an azimuthal scan, because of beam attenuation and multiple-scattering (dynamic) effects (see below).

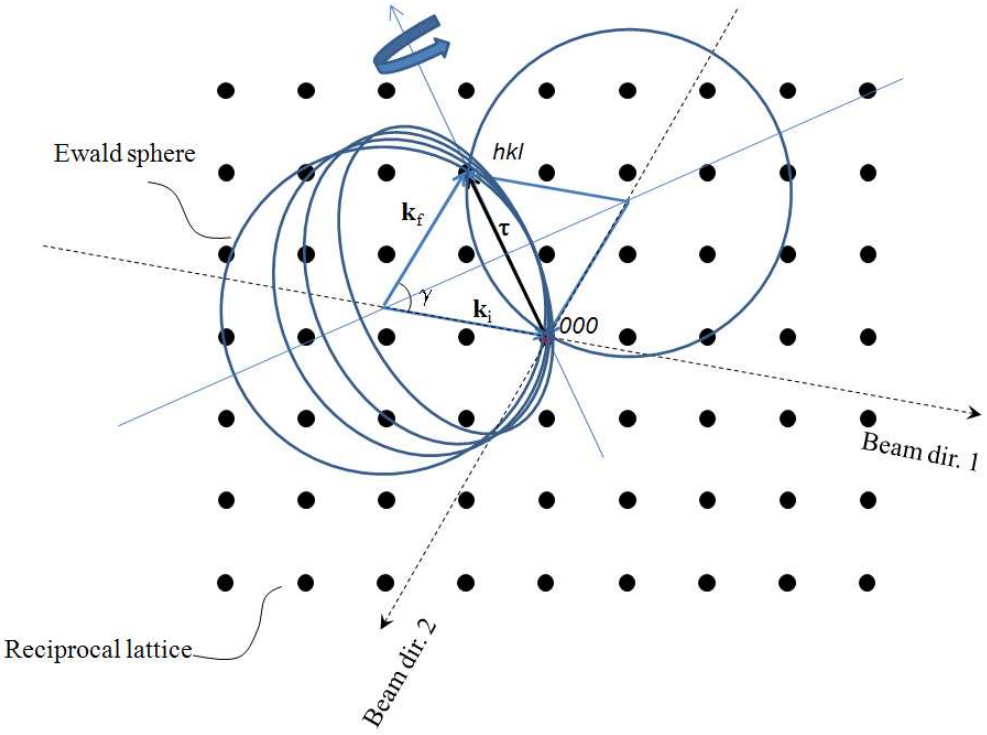

Figure 3: Ewald construction illustrating how Bragg scattering conditions are maintained during an azimuthal scan.

5.1.3 Four-circle diffractometry

For single-crystal experiments with monochromatic radiation, it is quite apparent that one should strive to maintain the maximum flexibility in orienting the crystal. One way to accomplish this is to mount the crystal in an *Eulerian cradle*, as illustrated in fig. 4 (note the alternative nomenclature for the angles). The whole assembly, including the detector arm, is known as a **four-circle diffractometer**. With a four-circle diffractometer, one can in principle (barring mechanical collisions and shadowing effects) access all nodes of the reciprocal space that are accessible for a given wavelengh. It is an easy exercise in the Ewald construction (left to the reader) to show that the accessible nodes are contained within a sphere of radius $4\pi/\lambda$, centered on the origin of reciprocal space. This is equivalent to saying that **the shortest accessible d-spacing is 1/2 the wavelength** — a statement that can be easily verified from Bragg law by setting θ to have its maximum value (90° in backscattering; the $\lambda/2$ limit is often referred to as the **Bragg cut-off**).

Modern four-circle diffractometers often employ an alternative, more open geometry, known as κ **geometry**; here the κ-axis, which replaces the χ-axis, is not perpendicular to the Ω-axis, but forms an angle of approximately 60° with it.

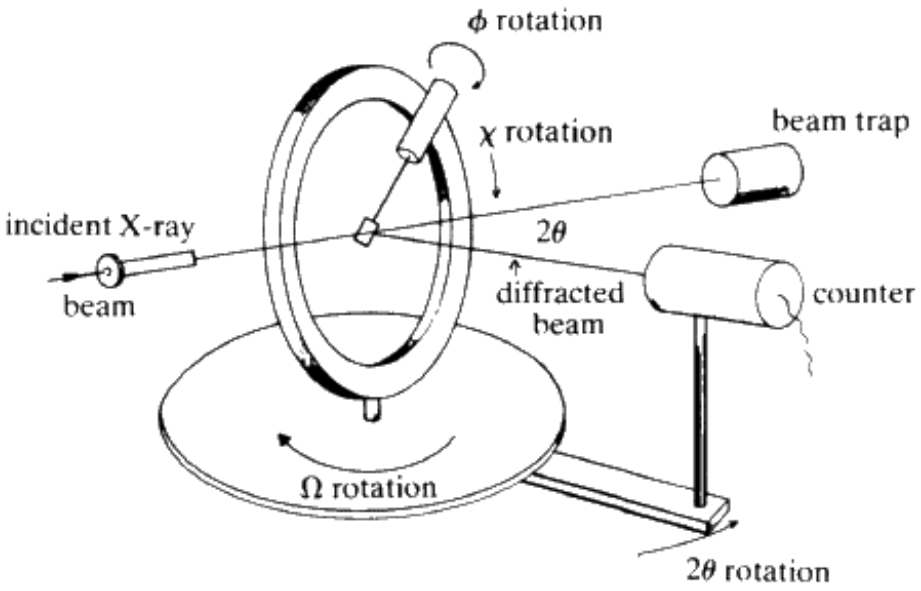

Figure 4: The geometry of a "four circle" single-crystal diffractometer. The "four circles" (actually four axes) are marked "ϕ", "χ", "Ω" and "2θ". The 2θ and Ω angles are also known as γ and η — a notation we will often employ in the remainder to avoid clutter and confusion with other symbols (e.g., the solid angle)

5.2 Powder diffraction

5.2.1 Debye-Scherrer cones

A "powder" sample is a more or less "random" collection of small single crystals, known as "crystallites". As explained more thoroughly in Appendix III, **the cross section for the whole powder sample depends on the *modulus* of the scattering vector q but not on its direction**. For a monochromatic incident beam, the 2θ angle *between* the incident and scattered beam is fixed for a given Bragg reflection, but, as we just said, the angle *around* the incident beam is arbitrary. It is easy to understand that the *locus* of all the possible scattered beams is a **cone** around the direction of the incident beam.

For monochromatic powder diffraction, the scattered beams form a series of cones (fig. 5), known as Debye-Scherrer cones (D-S cones in the remainder), one for each "non-degenerate" (see below) node of the reciprocal lattice.

It follows naturally that all the symmetry-equivalent RL nodes, having the same q, *contribute to the same D-S cone*. This is also illustrated by the Ewald construction in fig. 6. Moreover, *accidentally degenerate* reflections, having the same q but unrelated hkl's, also contribute to the same D-S cone. This is the case for example, for reflections $[333]$ and $[115]$ in the cubic system, since $3^2+3^2+3^2 = 1^2+1^2+5^2$.

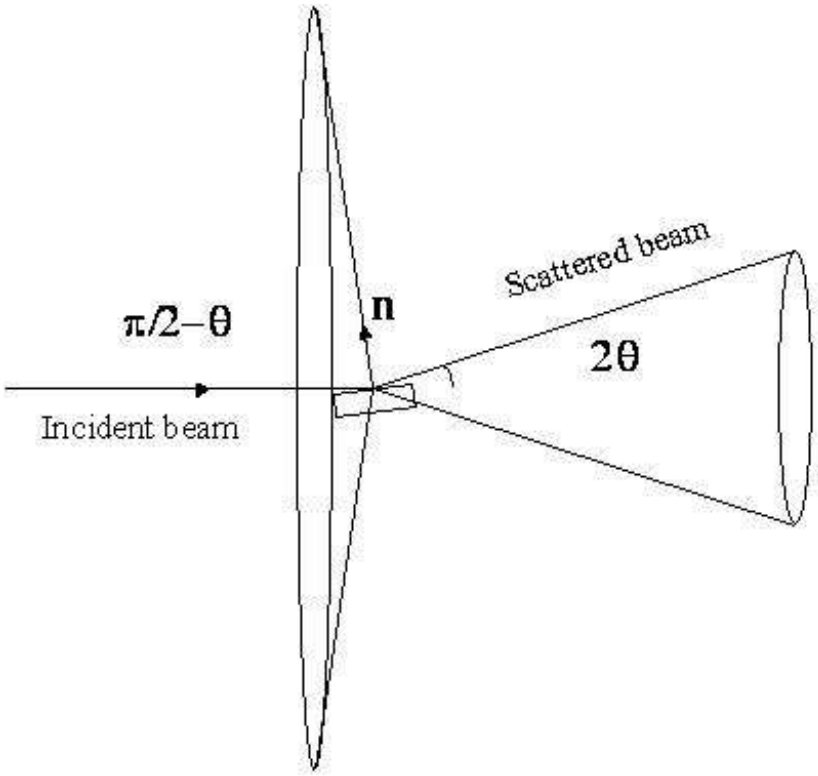

Figure 5: Debye-Scherrer cones and the orientations of the sets of Bragg planes generating them.

5.2.2 The Debye-Scherrer geometry

The Debye-Scherrer geometry employs a **parallel beam**, and the sample has a roughly cylindirical symmetry. The sample is contained in a tube (neutrons) or capillary (x-rays), and is uniformly illuminated by the incident beam. The detector(s) are placed on a ”detection cylinder” (fig. 7, generally covering only a small portion of the cylinder, near the scattering plane. The typical set-up used for laboratory x-ray diffraction employs a single detector, and a series of slits (often of the multi-lamellar type, known as “Soller slits”) to define the incident and scattered beam directions. The main advantage of this geometry is that it is easy to rotate the sample around its axis, thereby obtaining a good powder average and eliminating at least part of the non-randomness of the real powder sample (**preferred orientation**). Also, geometrical aberrations on the Bragg peak positions can be reduced or eliminated by employing Soller slits. Therefore, the Debye-Scherrer geometry is generally employed to obtain quantitative intensity measurements. Another advantage of this geometry is that it is easy to use many detectors simultaneously, as it is done in reactor-based neutron diffractometers, such as D20 and D2B at the ILL (see feig. 7. There are several variants of the Debye-Scherrer geometry, differing mainly for the degree and type of collimation, the type of monochromator and the detector technology. An important class of instruments, for both x-rays and neutrons, employs a linear position-sensitive detector (PSD) without scattered-beam collimation. This results in a very large increase of count rates, at the expense of introducing some aberrations. Another important variant is the analyser geometry,

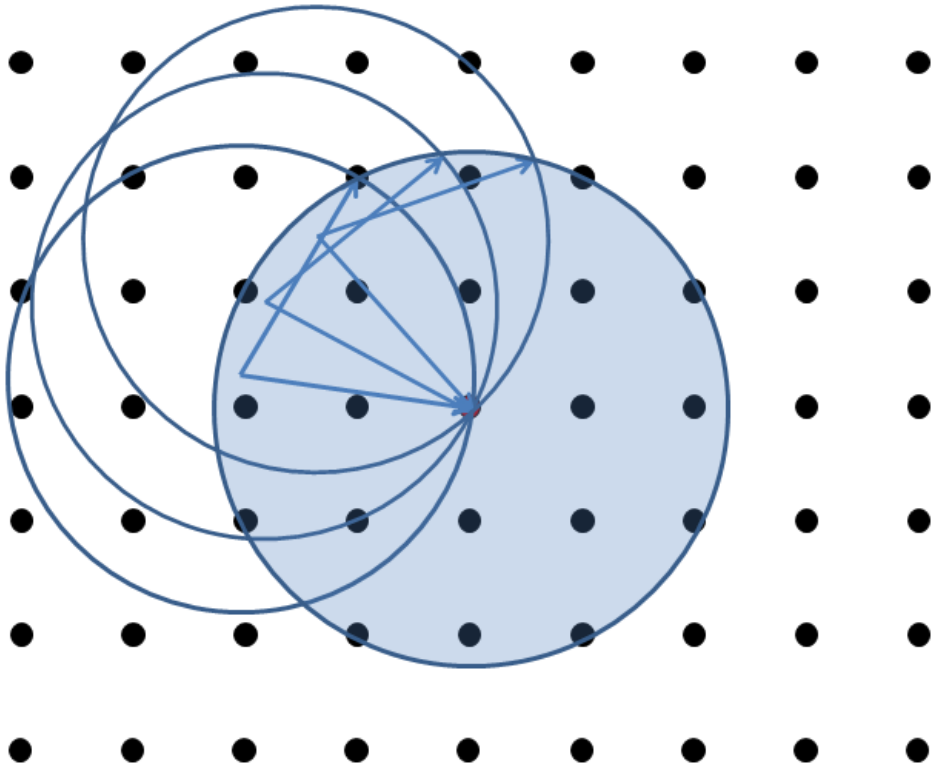

Figure 6: Ewald construction for powder diffraction, to represent the crystal being rotated randomly around the direction of the incident beam (the figure actually shows the opposite, for clarity).

where the Soller slits on the scattered beam are replaced with an analyser crystal. This results in a considerable intensity loss, but with a much-enhanced resolution and precision. The analyser geometry is frequently employed at synchrotron sources, coupled with a parallel incident beam. Fig. 8 shows a comparative example of X-ray and neutron high-resolution data collected on the same compound using variants of the the Debye-Scherrer geometry.

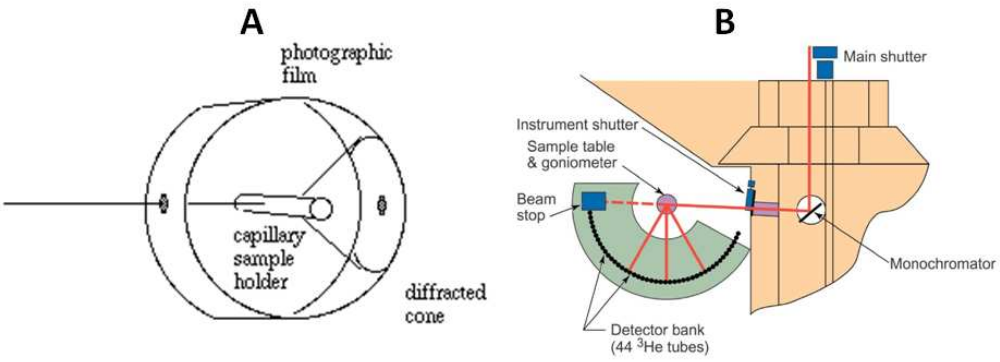

Figure 7: The Debye-Scherrer powder diffraction geometry, as implemented on a film camera (**A**) and on a modern constant-wavelength powder diffractometer (**B**). Note that, in the latter, the film has been replaced with an array of ^3He gas tubes.

Key points to retain about powder diffraction

- **In powder diffraction methods, the intensity around the D-S cones is *always integrated*, yielding a 1-dimensional pattern.**
- **Powder diffraction peaks are usually well-separated at low q, but become increasingly crowded at high q often becoming completely overlapped. This substantially reduce the amount of information available to solve or refine the structure precisely (see below).**

6 Profiles and integrated intensities

In all the techniques mentioned in the previous sections, one measured either a certain number of "counts" in the detector ("counting" detectors) or a continuous variable (e.g., the "blackening" of a photographic film, the amount of charge stored in a Charge-Coupled Device (CCD) or in an image plate, etc). Provided that the detector is well designed, it is possible to recover this value quantitatively and employ it to learn something about the crystal structure (see below). As we have seen in the previous example, the detected intensity comes in the form of **spots**, **rings** or **1-dimensional peaks**, depending on the technique one employs. With linear position-sensitive detectors or area detectors, the scattered intensity is in general distributed among more than one "pixel" or "bin".

When dealing with diffraction data from crystalline matter, one is in general left with two choices:

- **Sum up the pixels or bins pertaining to a single node of the RL, obtaining the so-called *integrated intensity*. This is the method of choice for *single-crystal diffraction*. As one can perhaps guess from eq. 10, *the integrated intensity is proportional to the squared modulus of the structur factor, but with some important geometrical factors.***
- **Retain the separate pixels and analyse the *profile* of the peaks. This is the method of choice for *powder diffraction*, where peak overlap prevents unambiguous assignment of the intensity to a single RL node. In this case, single-node integrated intensities are extracted as part of the analysis.**

In either case, an essential step in the quantitative analysis of diffraction data is **to calculate integrated intensities from the expression of the cross section (eq. 10)**.

The calculation is slightly different for different experimental geometries, but in all cases **it always involves converting the 3-dimensional δ- function in eq. 10 into appropriate polar**

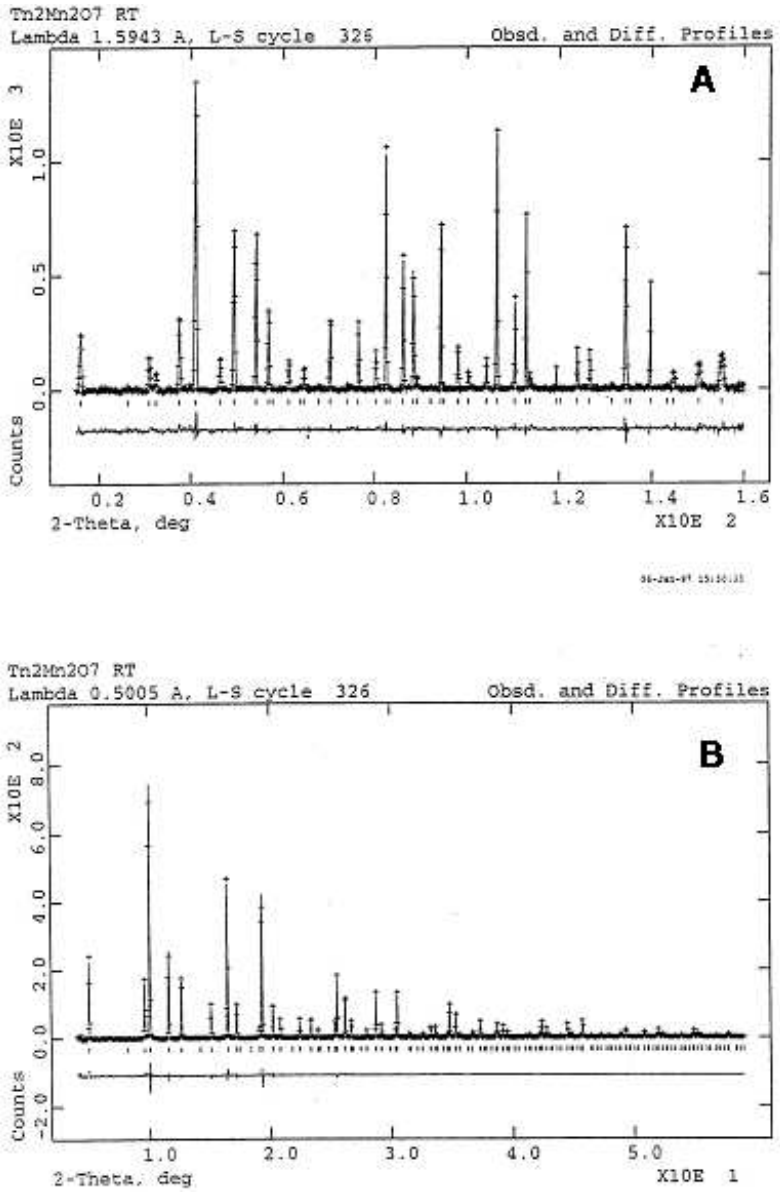

Figure 8: X-ray and neutron high-resolution powder diffraction at a glance. **A**: neutron powder diffraction (D2B-ILL, Grenoble, France, $\lambda = 1.594$) and **B** synchrotron x-ray diffraction (X7a-NSLS, Brookhaven, USA, $\lambda = 0.5000$) data on the pyrochlore compound $Tl_2Mn_2O_2$. Both instruments employ variants of the Debye-Scherrer geometry. Note how the intensity decays at high q much more for the X-ray data, due to the X-ray form factor. The structure is cubic, and peak overlap is minimal for the neutron data, but it is clearly visible at high q for the X-ray data, collected with a much shorter wavelength. Both data sets are fitted using the **Rietveld method** (see below)

coordinates, followed by integration over some of the variables. Calculations for different experimental geometries are provided in **Appendix III**.

The key point to remember are the following

- **The integrated intensity can always be reduced to a dimensionless quantity (counts).**
- **The general expression for the integrated intensity (number of particles) is**

$$P_{\boldsymbol{\tau}} = N_c \left(\frac{d^3}{v_0}\right) m_{\boldsymbol{\tau}} \left|F(\boldsymbol{\tau})\right|^2 \mathcal{P}(\gamma)\mathcal{L}(\gamma)\mathcal{A}_{\boldsymbol{\tau}}(\lambda,\gamma)\mathcal{F}_{inc} \tag{25}$$

where

- N_c **is the number of unit cells in the sample.**
- d **is the d-spacing of the reflection.**
- v_0 **is the unit-cell volume.**
- $m_{\boldsymbol{\tau}}$ **(powder diffraction only) is the *number of symmetry-equivalent reflections*. This accounts for the fact that in powder diffraction these reflections are not separable, and will always contribute to the same Bragg powder peak (see previous discussion and fig. 6.**
- $\mathcal{P}(\gamma)$ **is the *polarisation factor* (dimensionless), which we have already introduced.**
- $\mathcal{L}(\gamma)$ **is the so-called *Lorentz factor* (dimensionless), and contains all the experiment-specific geometrical factors arising from the δ-function integration.**
- $\mathcal{A}_{\boldsymbol{\tau}}(\lambda,\gamma)$ **(dimensionless) is the *attenuation and extinction coefficient*, which account for the beam absorption and for dynamical effects.**
- $\mathcal{F}_{inc}$ **is the incident time-integrated flux term (counts per square metre), which accounts for the strength of the incident beam and for the counting time.**

In exam problems, the intensities will be usually corrected for the Lorentz, polarisation, attenuation and incident flux terms, but the role these terms may be requested as part of the discussion.

7 Structural solution from diffraction data

Diffraction data can be used for many purposes, including obtaining information about the microstructure, defects and other aspects of the crystal under investigation. In general, however, **crystallographers are primarily interested in solving the crystal structure, i.e., to determine where the atoms are**. This translates in trying to determine the "scattering density" (e.g., electron density) in the unit cell. As we shall see in this section, the main obstacle to this effect is the so-called *phase problem*. We will briefly outline what this problem is and some of the methods to solve it.

7.1 The phase problem

From eq. 4, we can see that **the structure factor is proportional to the Fourier transform of the charge density (or, more in general, scattering density) integrated over the unit cell**. By the elementary theory of the Fourier transform over a finite interval (extended to 3 dimensions) we can calculate the charge density given all the structure factors:

$$f(\mathbf{r}) = \frac{1}{r_0\, v_0} \sum_{\boldsymbol{\tau}} F(\boldsymbol{\tau}) e^{\boldsymbol{\tau}\cdot\mathbf{r}} \tag{26}$$

From eq. 26 follows that **if we were able to measure all the structure factors, we could reconstruct the charge density exactly**. Clearly, it is impossible to measure all the infinite nodes of the reciprocal space, but it can be shown that it would be sufficient to measure up to a value of q_{max} to obtain a ***Fourier map*** with **resolution** $2\pi/q_{max}$ in *real space*. Therefore, the limited number of measured reflections does not pose an insurmountable problem to the reconstruction of the charge density

Direct reconstruction of the charge density is impossible, because only the *amplitudes* of the structure factors are known (through the term $|F|^2$ in the cross section), while the *phases* are unknown. Solving a crystal structure is therefore equivalent to *phasing* the reflections.

7.2 Single-crystal methods of structural solution

7.2.1 The Patterson method

Given that the scattering density cannot be determined without phasing the reflections, it is nonetheless possible to obtain some degree of information about it without any knowledge of the phases. Again, from eq 4, we obtain easily:

$$|F(\boldsymbol{q})|^2 = r_0^2 \iint_{unit\,cell} d\boldsymbol{r} d\boldsymbol{r}' f(\boldsymbol{r}) f(\boldsymbol{r}') e^{-i\boldsymbol{q}\cdot(\boldsymbol{r}-\boldsymbol{r}')} \tag{27}$$

With a change of variable (left as an exercise) and some manipulations we obtain:

$$\frac{1}{r_0^2\, v_0} \sum_{\boldsymbol{\tau}} |F(\boldsymbol{\tau})|^2 e^{\boldsymbol{\tau}\cdot\mathbf{r}} = \int_{unit\,cell} d\boldsymbol{r}' f(\boldsymbol{r}') f(\boldsymbol{r}+\boldsymbol{r}') = P(\mathbf{r}) \tag{28}$$

The function defined in eq. 28 is known as the ***Patterson function*** (or "Patterson" for the cognoscenti, from Lindo Patterson, 1934). One can perhaps recognise in eq. 28 that the Patterson is **the autocorrelation function of the scattering density**.

Important properties of the Patterson function for atomic-like scattering densities

- **Patterson functions are 3-dimensional functions defined within one unit cell, and are usually presented in the form of 2-dimensional "slices".**
- **Atomic-like scattering densities are *mostly zero*, except at the atomic positions. Therefore the Patterson function will be mostly zero as well, except at the *origin* ($\boldsymbol{r} = 0$) and *for values of r corresponding to vectors joining two atoms*. At these vectors, the Patterson function will have peaks.**
- **The height of the $\boldsymbol{r} = 0$ peak can be easily calculated (left as an exercise).**
- **The height of the peaks for $r \neq 0$ is *proportional to the product of the scattering power of the two atoms joined by the vector r*. For example, for X-rays, the height of the Patterson peaks is $\propto Z^2$ for atoms of the same species and $\propto Z_1 Z_2$ for atoms of different species.**
- **If the crystal structure contains few heavy atoms and many light atoms, *one can easily see that the Patterson will be dominated by heavy-atom peaks*. The strongest family will be at r vectors joining two heavy atoms, and the next strongest the one at r vectors joining a heavy and a light atom.**
- **In simples cases, the Patterson can often be *uniquely interpreted*, yielding the exact position of all the atoms in the unit cell.**

7.2.2 Direct methods

If the scattering density was an arbitrary, complex function, solving *a priori* the phase problem would be impossible, since and infinite number of such functions would be compatible with a given set of $|F|^2$'s. However, *real* charge densities have three key properties that are extensively exploited by the so-called **direct methods** to "phase" the reflections, without any *a priori* knowledge of the crystal structure:

- Scattering densities are *real* functions (the imaginary anomalous term can be safely ignored,

except near a resonance)..

- Charge densities are *positive* functions. Note that **Fermi lengths in neutron scattering can be positive and negative**, but special direct methods have been developed to deal with these problems.

- Scattering densities are *"atomic-like"*. In other words, if one has the correct phases, one should get *peaks* in the Fourier maps, whereas if the phases are wrong, the Fourier maps consists of oscillations throughout the unit cell.

Direct methods exploit a number of inequalities existing between terms of the Fourier series for positive-definite functions, to yield "probable" phase relations between sets of reflections (*pairs*, *triplet* and *quartets*) based on the ratios of their intensities. Direct methods are very effective in solving moderately complex structures without any prior knowledge, and even macromolecular structures are not out of reach for these methods.

Direct methods usually proceed in an iterative manner. After a first attempt to "phase" the reflections, Fourier maps are calculated ("Fourier recycling") and the crystallographer (or, increasingly, the software) attempts to identify "atoms" in the maps. These are then employed to obtain a more precise "phasing" in the next step.

7.2.3 Structural "optimisation": least-square refinements

In general a certain degree of prior knowledge is always present before one attempts to solve a crystal structure. For example, the stoichiometry and the number of formula units in the unit cell (known as "Z") are almost always known. For molecular crystals, the molecular connectivity and the shape of its rigid components is also known, and structure solutions entails the determination of the flexible parts ("torsion angles") and of the packing and orientation of the molecules within the unit cell. All this knowledge must be exploited by any good structural solution method. Two strategies are usually adopted:

- If the information is fragmentary, one can incorporate it in the direct method approach, yielding more precise phase relations.

- If one is reasonably close of the solution, with only a few free parameters left to determine, it is possible to *minimise the agreement between observed and calculated squared structure factors* $|F|^2$ *as a function of the free parameters*. This is clearly a non-linear optimisation problem, and a number of strategies have been developed to solve it in a variety of cases.

Most problems in physical crystallography involve determining subtle structural variations from well-known and rather simple structural motifs. Therefore, structural optimisation is usually the method of choice for the structural condensed-matter physicist.

7.3 Powder data and the Rietveld method

All the structural solution techniques described above for single crystal diffraction have been adapted to powder diffraction, including the Patterson method and the direct methods. Clearly, one has to contend with the much greater **degeneracy** of powder data, which, as we have seen, are "compressed" into one dimension. Among the powder methods, one stands out by far, being almost ubiquitous in all applications: **the Rietveld methods** , discovered by the Dutch crystallographer Hugo Rietveld in 1969.

In the Rietveld method, one performs a nonlinear least-square fit *of the measured profile*, rather than of the $|F|^2$ as in the single-crystal methods. This could appear more complicated, since one has to fit the microstructural and instrumental parameters controlling peak broadening and the background at the same time, but has the great advantage of *accounting automatically for peak overlap*. This is illustrated in fig. 8.

8 Beyond the small-crystal approximation: dynamical diffraction and extinction

Up to this point, we have developed the diffraction formalism **strictly in the kinematic approximation**, i.e., **ignoring completely the interaction of the scattered beam with the crystal and the interference between the forward-scattered beam and the incident beam**. Taking this into account, in the so-called **full dynamical diffraction theory**, results in a series of rather unusual phenomena, the most peculiar of which are observable only in highly perfect crystals. A full treatment of the problem is much beyond the scope of this course. Here, we will only see a brief description of the way these effects were described for the first time by Darwin (1914) in two famous papers, with the aim of understanding how our approximations need to be relaxed. We will also give a qualitative description of two important effects: **extinction** and **anomalous transmission (the Borrmann effect)**. For a full quantitative treatment, see [6]

8.1 The Darwin treatment of dynamical effects

The starting point of Darwin's treatment of dynamical effects is **the calculation of the scattering amplitude (electric field for X-rays) due to an entire plane of atoms**. In order to get correct quantitative results, **it is extremely important to relax the far-field approximation that we have employed so far**, and employ a realistic geometry, as shown in fig. 9

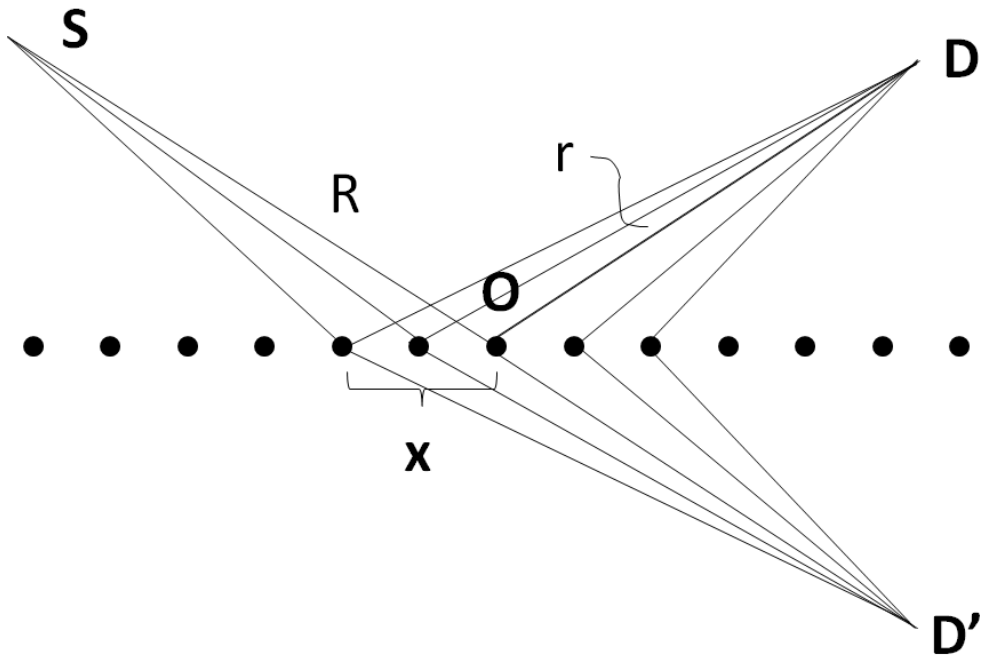

Figure 9: The Darwin construction is the starting point to calculate dynamical effects in extended crystals. The beam is emitted by the source **S** (its distance from the origin being R) and scattered by a 2-dimensional array of atoms towards the "detector" **D** (distance r to the origin), as well as forward-scattered towards the point **D'** (also distance r to the origin). No far-field approximation is made, so all the paths are calculated up to the quadratic term in **x**.

It can be shown (see, for example, [4], p. 318) that

$$\begin{aligned} E_D &= 2E_0 r_0 dM\, f(q) e^{-i[q\,(R+r)-\omega t]} e^{i\pi/2} \\ E_{D'} &= 2E_0 r_0 dM\, f(0) e^{-i[q\,(R+r)-\omega t]} e^{i\pi/2} \end{aligned} \tag{29}$$

In eq. 29, M is the number of atoms per unit area and d is the d-spacing. The similarity between the two expressions is due to the fact that all the path lengths are the same. **Here, for the first time, we see that the real scattered amplitude is proportional to the *density* of scatterers (M), *not* to the total number of atoms — a result that signals a clear departure from the kinematic approximation.**

Even if we have not deduced eq. 29 explicitly, we can notice one important aspects:

The reflected and forward-scattered beams suffer a phase shift of $\pi/2$ with respect to the incident beam. This is important, because a beam that has reflected *twice* will be $180°$ degree out of phase, and this is the main contribution to the reduction of the primary beam intensity, as required by the conservation of energy (which is not obeyed in the kinematic approximation)

Darwin's calculation then proceeds according to the schema shown in fig. 10. Essentially, one sums up the contributions from the different layers, both in **transmission** and **close or at Bragg reflection conditions**, each with the appropriate amplitude and phase (here, one can also take into account absorption effects).

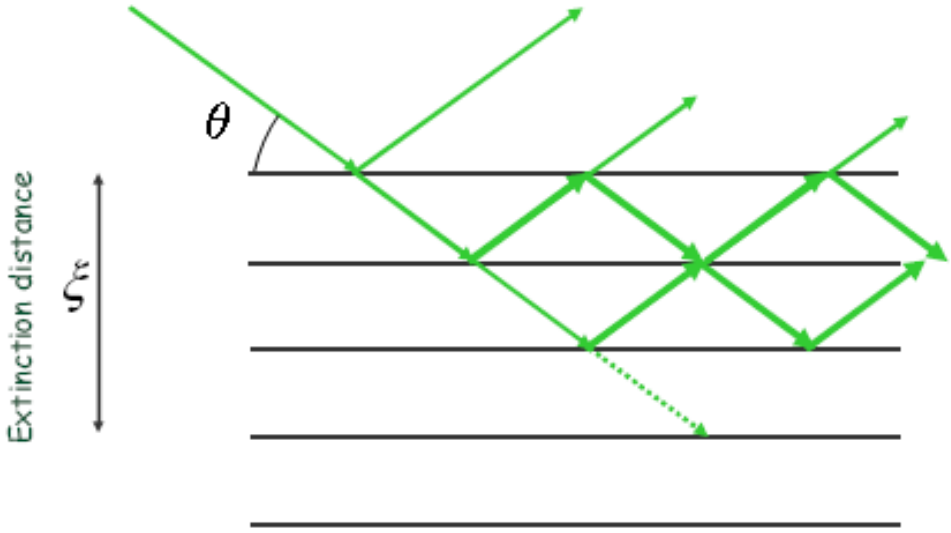

Figure 10: The Darwin construction extended to the full 3-dimensional crystal. We here consider the case of a crystal cut *parallel* to the Bragg planes under investigation, the beam making and angle θ with the surface.

The most significant results that can be obtained with the Darwin construction are:

- **In *transmission* one can calculate the *refractive index for X-rays***

$$n = 1 - r_0 \frac{N\lambda^2 Z}{2\pi} < 1 \tag{30}$$

where N is the number of atoms per unit volume and Z is the atomic number. On the basis of this important result, one can predict *total external reflection* of X-rays from materials surfaces — a key result at the basis of the *X-ray reflectivity technique*.

- **In *Bragg reflection* (without absorption) one finds that the X-ray beam *suffers total reflection* within an angular region**

$$|\theta - \theta_{Bragg}| < r_0 \frac{N\lambda^2 f(q)}{\pi \sin 2\theta} = s \tag{31}$$

where again, N is the number of atoms per unit volume. The angle s is known as the *Darwin width*. Outside this "total reflection" region, the scattered intensity decays polynomially (fig. 11). We find, here, the important result that in a perfect infinite crystal *the width of the Bragg peaks is not a delta function, but is finite, and is given by the Darwin width*.

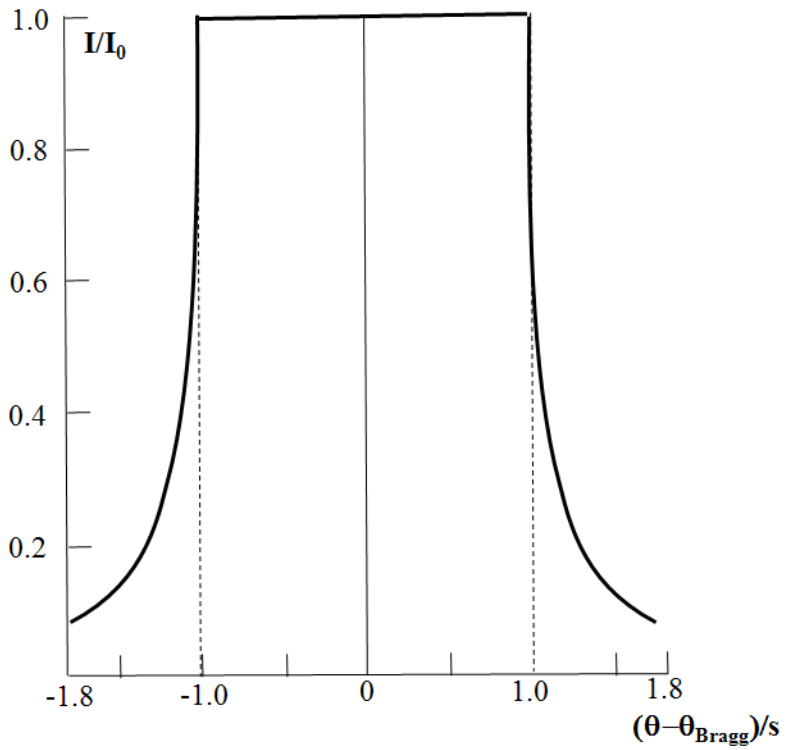

Figure 11: The Darwin peak profile in the case of a symmetrically cut crystal without absorption. The parameter s is defined in eq. 31. The interval -1 to 1 is the region of total reflection.

8.2 Extinction

From the discussion in the previous section one can deduce two important facts about the Bragg peaks intensity from a perfect crystal:

- **When the full dynamic theory is applied, the integrated intensity of each Bragg peak is always *lower* than expected from the kinematic theory — a phenomenon known as *extinction*. Although this reduction is not immediately apparent from the equations we presented, it should be clear from the fact that *the most important consequence of the dynamical theory of scattering is to restore energy conservation*. We can think of this, intuitively, as if the scattered energy from each layer would be lost from the primary beam producing scattering from the next layer. Single crystal diffraction data *almost always* need to be corrected for extinction to yield realistic structure factors.**
- **In the full dynamic limit, *the integrated Bragg intensity is independent on the structure factor, and is instead proportional to the Darwin width*. Therefore, *diffraction data from large, highly perfect crystals are essentially useless to determine crystal structures*. Crystallographers even resort to "dunk" their crystals in liquid nitrogen to create a *mosaic* of smaller, slightly mis-oriented crystals to reduce extinction — these samples are known as *ideally imperfect crystals*.**

8.3 The Borrmann (anomalous transmission) effect

An extreme example of the dynamical diffraction phenomenology as differing from the kinematic theory expectations is provided by the **anomalous transmission effect, a.k.a. the Borrmann effect**, first discovered in 1941 in quartz by Gerhard Borrmann [5]. This phenomenon is illustrated in fig. 12. In the kinematic approximation, one would expect the transmitted beam to exit *directly opposite* to the entry point, and to be attenuated as:

$$I = I_0 e^{-\mu L} \tag{32}$$

where μ is the attenuation length (usually of the order of a few μm for X-rays) and L is the travelled distance. Instead, for highly perfect crystals, both Bragg scattered and transmitted beams exit **on the face directly opposite the entry face**. Both beams can be strong, much more so than expected, since they have apparently "travelled" several 10's of the "normal" attenuation length. The reason of this apparently bizarre result is that energy is transferred through the crystal by a **standing wave**, rather than by a normal travelling wave.

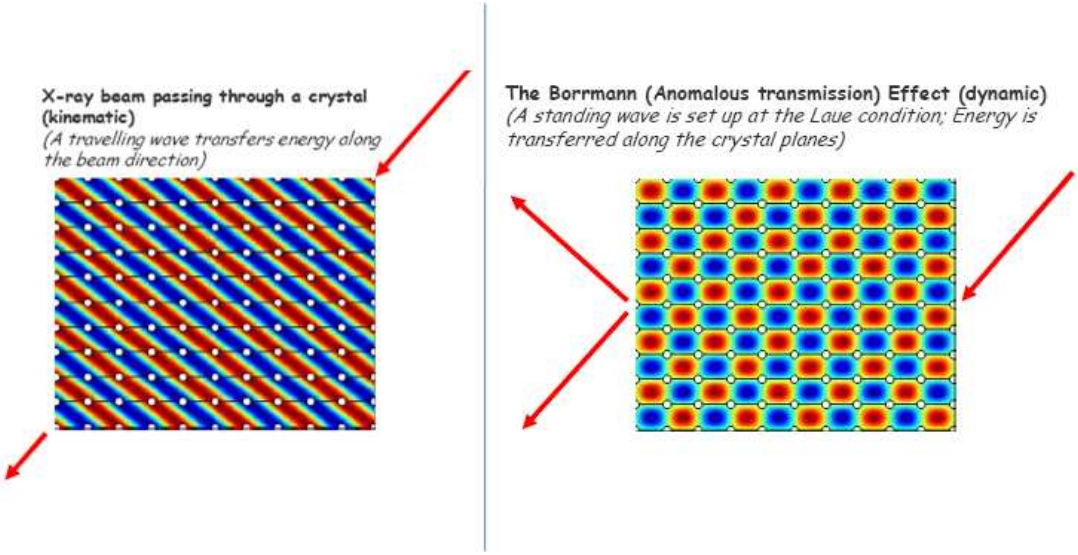

Figure 12: A beam of X-rays traversing a thick, perfect crystal. In the kinematic approximation (**left**), one expects the portion of the beam that is not absorbed to exit *directly opposite* to the entry point. Instead, one observes intense transmitted and scattered beams emerging from the face opposite to the entry face (**right**).

8.3.1 Pendellösung fringes

The intensity of the transmitted and diffracted beam vary strongly with the thickness of the crystal. In a tapered crystal (fig. 13), the intensities are modulated, giving rise to the so-called **Pendellösung fringes** (the name, coined by Ewald, means "spherical solution".)

The expression for the transmitted and scattered intensities are

$$\begin{aligned} I(T) &= I_0 \cos^2 \xi \\ I(S) &= I_0 \sin^2 \xi \\ \xi &= r_0 \frac{N\lambda f(q)\mathcal{P}}{\cos\theta} x \end{aligned} \tag{33}$$

Where $\mathcal{P}$ is a polarisation factor ($= 1$ or $= \cos 2\theta$ depending on whether the polarisation is parallel or perpendicular to the scattering plane), x is the thickness of the crystal and all other symbols have the usual meaning.

Eq. 33 raises an interesting possibility:

The X-ray form factors can be determined with great accuracy by observing the *spacing* of the Pendellösung fringes.

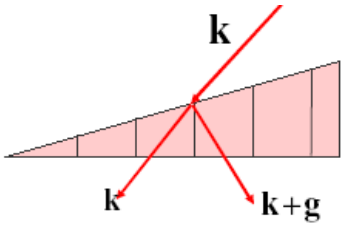

Figure 13: The setup to observe Pendellösung fringes (see text).

9 Appendix I: lattice planes and the "d-spacing"

By looking at fig. 14 we can convince ourselves of the following statements:

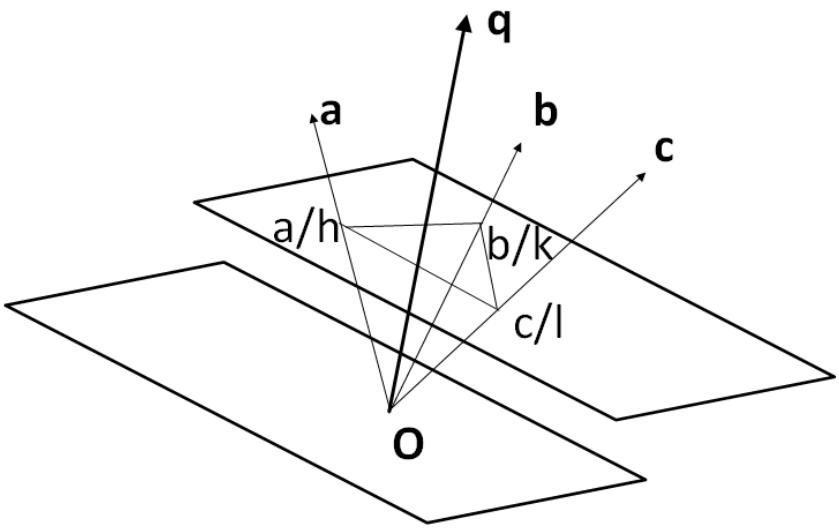

Figure 14: Construction employed to derive the connection between Bragg's law and the spacing between atomic layers (see text).

- For each pair of non-collinear lattice vectors, $\mathbf{u}$ and $\mathbf{v}$, defining a family of planes in real space, there is a RL vector $\mathbf{q}$ *perpendicular* to them. We can always ensure that the Miller indices of $\mathbf{q}$ have no common factors, so that $\mathbf{q}$ is the shortest such vector. Naturally, all integral multiples of $\mathbf{q}$ are also perpendicular to $\mathbf{u}$ and $\mathbf{v}$. This is very easy to prove — it is sufficient to show that the appropriate linear equations have a rational solution and divide by the common factors, if any.

- Given an arbitrary such plane passing through the origin (see fig. 14), the next plane in the family intercepts the coordinate axes at positions $1/h, 1/k, 1/l$. In fact, the three direct-lattice vectors $hk(\mathbf{a}_1/h - \mathbf{a}_2/k)$, $hl(\mathbf{a}_1/h - \mathbf{a}_3/l)$ and $kl(\mathbf{a}_2/k - \mathbf{a}_3/l)$ are all perpendicular to $\mathbf{q}$.

- The distance between adjacent direct-lattice planes belonging to the **u**–**v** family is $2\pi/q$. This is easily seen by projecting, for example, the intercept vector $\mathbf{a}_1/h$ onto $\mathbf{q}$, yielding $(2\pi h)/(qh) = 2\pi/q$. If we call this distance d — the **d-spacing**— then

$$d = 2\pi/q \tag{34}$$

Strictly speaking, eq. 34 is only valid for the shortest such RL vector, so in general $d = 2\pi n/q$ where n is an integer. Combining this with eq.22 we obtain the traditional formulation of **Bragg's law**:

$$2d \sin\theta = n\lambda \tag{35}$$

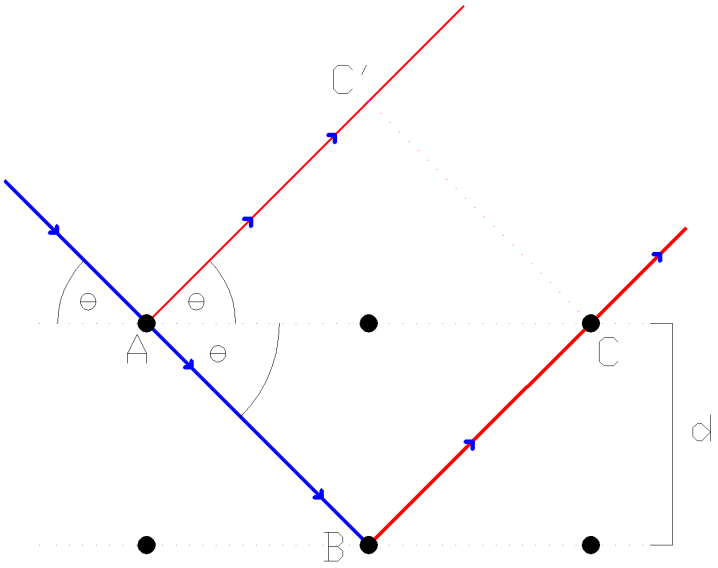

Figure 15: The traditional derivation of Bragg's law. The phase difference between waves reflected by the two adjacent planes is set to be $2\pi n$

In practice, the d-spacing is written using eq. 34 even for *higher order* reflections, and the "n" is almost always omitted in eq. 24. The more conventional derivation of Bragg's is depicted in fig. **??**, where the phase difference between waves specularly scattered by adjacent planes is set to a multiple of 2π.

10 Appendix II: more diffraction geometries

10.1 More single-crystal geometries.

10.1.1 The Laue geometry

The Laue geometry is the simplest diffraction geometry, and is this is the method used in the original discovery of X-ray diffraction by Max von Laue. Von Laue worked with two technicians, Walter Friedrich and his assistant Paul Knipping, to shine a beam of X-rays through a copper sulfate crystal and record its diffraction on a photographic plate. After being developed, the plate showed a large number of well-defined spots arranged in a pattern of intersecting ellipses around the spot produced by the central beam. Importantly, **the X-ray beam must not be monochromatised** — in fact, the Laue method uses mostly the continuous spectrum (bremsstrahlung) obtained by bombarding the anode with high-energy electrons. Various detector (or film) geometries can be employed, the most common being **transmission Laue** and **backscattering Laue**. The Laue geometry is still employed for a variety of applications, from orienting large single crystals of novel materials to the study of protein crystals with synchrotron radiation. Fig. 16 shows an example of transmission Laue from a protein crystal.

10.1.2 Time-sorted Laue geometry (neutrons)

The Laue geometry has a few disadvantages:

- The wavelength of the incident beam giving rise to each spot is not well defined, so it is very difficult to get accurate lattice parameters (one can readily obtain ratios of lattice parameters and lattice angles).
- For the same reason, higher-order peaks fall on top of each other — that is, 001, 002, 003 etc. contribute to the same spot on the detector. Their intensities cannot be deconvoluted, making quantitative analysis somewhat more difficult.

The time-sorted Laue method, as applied to time-of-flight neutron diffraction, solves both problems, in that the wavelength of each detected neutron is automatically measured by the time-of-flight method. An example of a modern time-sorted Laue camera is shown in fig. 17. The same method could be implemented with X-rays using a multi-channel (energy analyser) area detectors. Unfortunately, detectors of this kind are only at the prototyping stage.

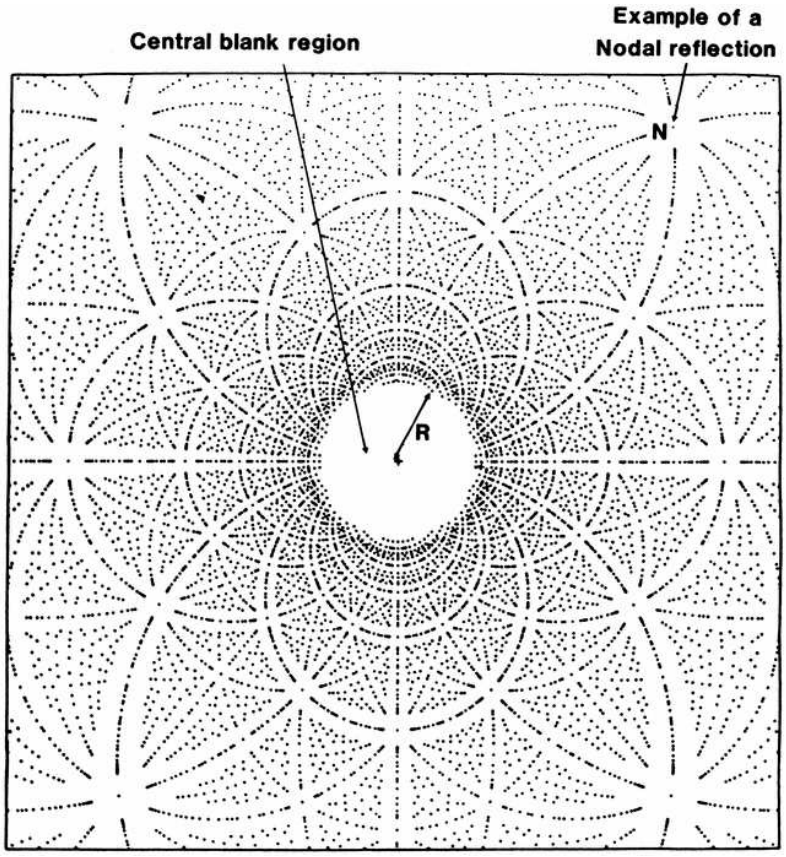

Figure 16: An example of a transmission Laue (simulated data) from a protein crystal. The spots on the elliptical paths belong to the same *zone*, i.e., plane in reciprocal space. "Nodal" reflections are low-order reflections.

10.2 More powder diffraction geometries.

10.2.1 More angle-dispersive techniques

Here, one employs **monochromatic** radiation, and the different Bragg peaks are accessed by varying the scattering angle 2θ.

A few more powder diffraction geometries are shown in fig. 18

Bragg-Brentano geometry This geometry employs a planar sample, with the normal axis coinciding with the direction of the scattering vector. (fig. 18 **B**). Since the direction of the normal axis has to vary as a function of 2θ, one can only employ a single detector or a small Position-Sensitive Detector (PSD). However, this geometry has many advantages, especially in the case of absorbing samples: in fact, the illuminated area of the sample can be much larger than the penetration depth, which results in a much increased effective sample volume with respect to the Debye-Scherrer geometry. This is further enhanced, in the case of laboratory diffractometers, by the so-called "parafocussing effect", so that the

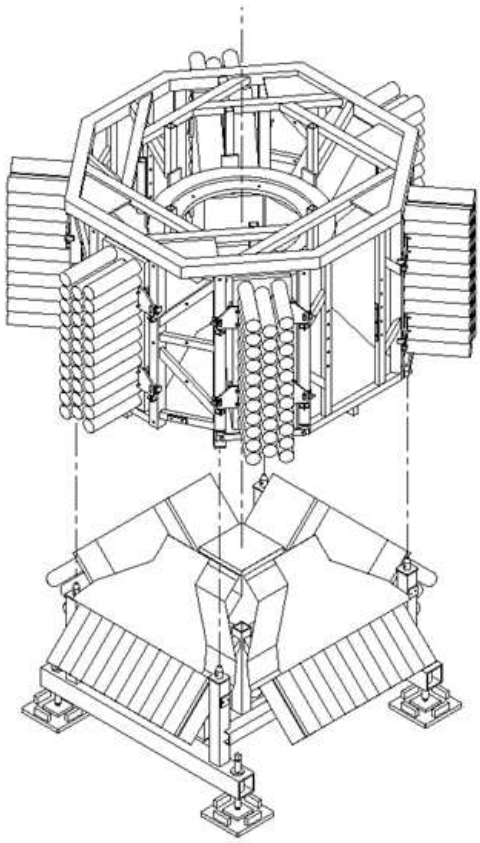

Figure 17: The time-sorted Laue camera installed on the SXD instrument at the ISIS facility (oxfordshire). The tubes are photo-multipliers that detect the light produced by the scintillator detectors array. The polychromatic neutron beam (not shown) comes from the left side of the picture.

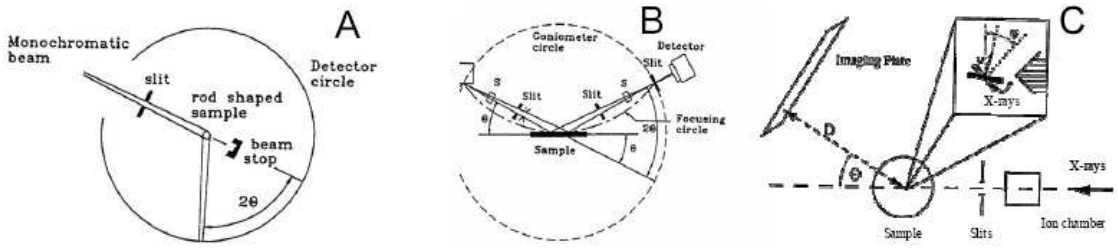

Figure 18: Three types of powder data acquisition geometries: A) Debye-Scherrer; B) Bragg-Brentano; C) Image-plate

pattern resolution becomes independent on the sample size. Also, the absorption correction is independent on 2θ. On the down side, spinning a flat plate is less effective in reducing systematic and statistical errors on the intensity. Therefore, this geometry is employed for

rapid data acquisition with a small detector solid angle, especially for absorbing samples.

Image plate geometry The sample is ideally a small sphere (fig. 18 **C**). The detector is replaced with a photo-sensitive plate, which is sensitised by the x-rays (or neutrons) and later "read" with a laser scanner. This is typically an uncollimated geometry, and, as such, prone to aberrations. However, it can collect full D-S cones for a large part of the diffraction pattern, especially at high energy, where the pattern is limited to low angles. The main disadvantage is that the plate read-out is slow. It is very popular at synchrotron sources, where is often coupled with scanning "masks" to obtain different patterns, for example at different temperatures, on the same image plate. Another important application is for high-pressure powder diffraction.

11 Appendix III: derivation of integrated intensities

11.1 Integrated intensities from a small single crystal

We start from the scattering cross section for a single crystal in the kinematical approximation (eq. 8, we have omitted the polarisation factor for simpicity and to deal with the general case of X-rays, neutrons and electrons), and ignore, for the moment, the intrinsic width of the peaks in reciprocal space.

$$\frac{d\sigma}{d\Omega} = N_c \frac{(2\pi)^3}{v_0} \sum_{\boldsymbol{\tau}} \delta(\mathbf{q} - \boldsymbol{\tau}) \left|F(\boldsymbol{\tau})\right|^2 \tag{36}$$

where $N_c = V/v_0$ in the number of unit cells in the crystal (or the "effective volume", if we take into account attenuation), and v_0 is the unit cell volume. The summation is over all the nodes $\boldsymbol{\tau}$ of the reciprocal lattice (RL). We now use the transformation properties of the 3-dimensional Dirac function.

$$\delta(\mathbf{q}) = \frac{\delta(\bar{q})\delta(\bar{\alpha})\delta(\bar{\chi})}{q^2 \sin\alpha} \tag{37}$$

We have used spherical coordinates with a z axis parallel to the beam, α and χ being the polar angles defining the direction of $\mathbf{q}$. We have also used the notation $\bar{q} = q - \tau$, $\bar{\alpha} = \alpha - \alpha_\tau$, $\bar{\chi} = \chi - \chi_\tau$, etc. to indicate that the delta functions are centered at the RL positions. We can use the construction in fig. 19 to relate "polar" angle α with the scattering angle γ. One can see from the figure that the polar angle χ coincides with the angle between the scattering plane and the horizontal plane. The relation is as follows:

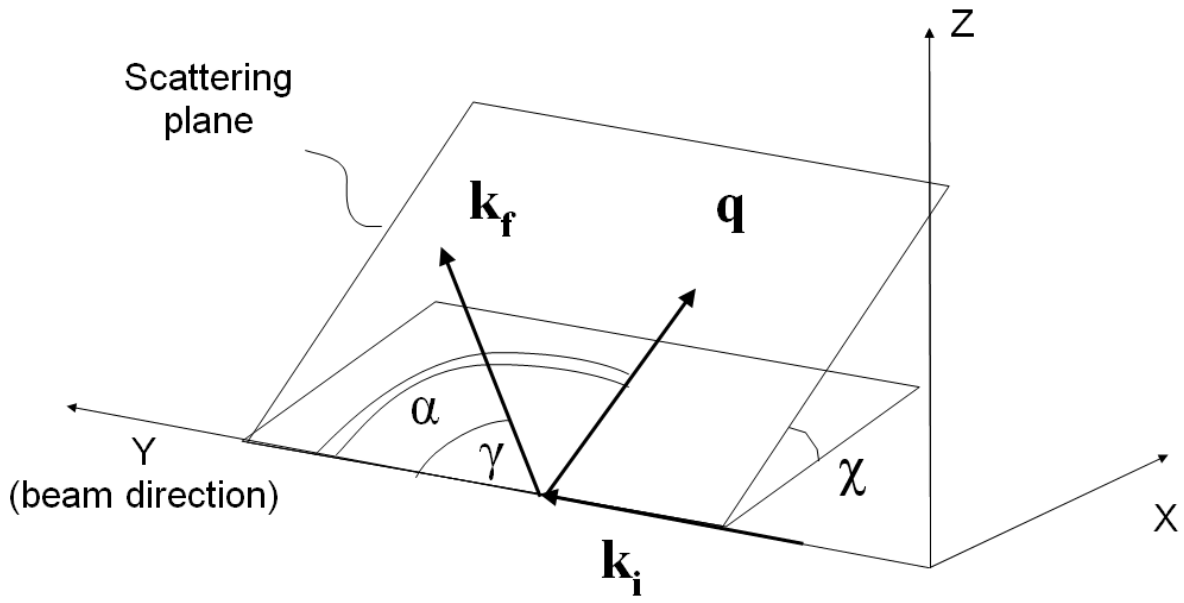

Figure 19: Construction showing the relation between the "polar" angle α and the scattering angle γ.

$$\begin{aligned} \alpha &= \frac{\pi+\gamma}{2} \\ \delta(\bar{\alpha})\,\delta(\bar{\chi}) &= 2\delta(\bar{\gamma})\,\delta(\bar{\chi}) \end{aligned} \tag{38}$$

With eq. 37 and 38, eq. 36 becomes:

$$\frac{d\sigma}{d\Omega} = N_c \frac{(2\pi)^3}{v_0} \sum_{RL} \frac{2\delta(\bar{q})\delta(\bar{\gamma})\delta(\bar{\chi})}{q^2\cos(\gamma/2)} \left|F(\boldsymbol{\tau})\right|^2 \tag{39}$$

11.1.1 Wavelength-dispersive case

We will start with the case of a wavelength-dispersive experiment, which easier to understand, and is relevant for Laue and time-sorted Laue diffraction.

We can first integrate eq. 39 over the detector solid angle $d\Omega = \sin\gamma d\gamma d\chi$, which we now assume to be centred on a *single* Bragg reflection. Doing the usual replacement $\gamma = 2\theta$ we obtain:

$$\begin{aligned} \frac{d\sigma}{d\Omega} &= N_c \frac{(2\pi)^3}{v_0} \frac{2\delta(\bar{q})\sin 2\theta_{\boldsymbol{\tau}}}{q^2\cos\theta_{\boldsymbol{\tau}}} \left|F(\boldsymbol{\tau})\right|^2 \\ &= N_c \frac{(2\pi)^3}{v_0} \frac{4\delta(\bar{q})\sin\theta_{\boldsymbol{\tau}}}{q^2} \left|F(\boldsymbol{\tau})\right|^2 \end{aligned} \tag{40}$$

To calculate the integrated cross section we can convert q to wavelength using

$$\begin{aligned} q &= \frac{4\pi \sin\theta}{\lambda} \\ \delta(\bar{q}) &= \frac{\lambda^2}{4\pi \sin\theta}\delta(\bar{\lambda}) \end{aligned} \tag{41}$$

yielding

$$\begin{aligned} \frac{d\sigma}{d\Omega} &= N_c \frac{(2\pi)^3}{v_0} 4 \sin\theta\lambda\, \delta(\bar{\lambda}) \frac{\lambda^3}{(4\pi \sin\theta)^3} \left|F(\boldsymbol{\tau})\right|^2 \\ &= N_c \frac{d^3}{v_0} 4 \sin\theta\lambda\, \delta(\bar{\lambda}) \left|F(\boldsymbol{\tau})\right|^2 \end{aligned} \tag{42}$$

where we have used Bragg's law

$$2d \sin\theta = \lambda \tag{43}$$

To get the scattered count rate $P_{\boldsymbol{\tau}}$, i.e., the number of scattered particles per second measured over the *whole* detector, we multiply by the **incident flux density** $\Phi(\lambda)$, so that the number of particles per square metre per second in the interval between λ and $\lambda + d\lambda$ is $\Phi(\lambda)d\lambda$, and integrate, obtaining

$$P_{\boldsymbol{\tau}} = N_c \frac{d_{\boldsymbol{\tau}}^3}{v_0} \left|F(\boldsymbol{\tau})\right|^2 \, 4 \sin\theta_{\boldsymbol{\tau}} \lambda_{\boldsymbol{\tau}} \Phi(\lambda_{\boldsymbol{\tau}}) \tag{44}$$

Although SI units can of course be used, one can see that eq. 44 is still correctly dimensioned if one expresses the wavelength in Ångstroms, the incident flux density in particles per square cm per second per Ångstrom and $\left|F(\boldsymbol{\tau})\right|^2$ in Barns — these are the more customary units employed in scattering experiments.

Eq. 44 can be modified empirically to account for beam attenuation effects through the crystal, by assuming that, at each wavelength λ, $N_c A_{\boldsymbol{\tau}}(\lambda)$ unit cells will contribute to the scattering, so that

$$P_{\boldsymbol{\tau}} = N_c \frac{d_{\boldsymbol{\tau}}^3}{v_0} \left|F(\boldsymbol{\tau})\right|^2 \, 4 \sin\theta_{\boldsymbol{\tau}} A_{\boldsymbol{\tau}}(\lambda) \lambda_{\boldsymbol{\tau}} \Phi(\lambda_{\boldsymbol{\tau}}) \tag{45}$$

The **attenuation coefficient** $A_{\boldsymbol{\tau}}(\lambda)$ is, in general, wavelength dependent and depends also on the shape of the crystal and on the scattering geometry. $A_{\boldsymbol{\tau}}(\lambda)$ is usually calculated by a finite-element method or by approximating the shape of the crystal to that of a sphere of cylinder, for

which analytical expressions have been developed. One can account for **extinction** in much the same way.

Referring to eq. 25, we can find the following expressions for the **Lorentz** factor $\mathcal{L}$ and the incident time-integrated flux $\mathcal{F}_{inc}$ (t is the total measuring time).

$$\begin{aligned} \mathcal{L} &= 4\sin\theta \\ \mathcal{F}_{inc} &= \lambda\Phi(\lambda)\,t \end{aligned} \tag{46}$$

11.1.2 Constant wavelength case

We start again from eq. 39 and analyse the Ewald construction in fig. 20. We can observe that this time we have the following reflection conditions:

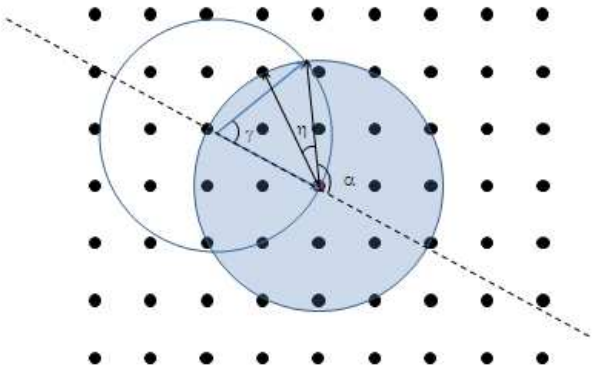

Figure 20: Ewald construction for the constant-wavelength case. The angle of rotation η is the rotation angle of the crystal required to bring the spot indicated by the arrow into scattering conditions.

- The *length* of the scattering vector **q** must correspond to the length of the RL vector under consideration. At constant wavelength, this is a condition on γ, namely:

$$q_{\boldsymbol{\tau}} = \frac{4\pi\sin\gamma/2}{\lambda} \tag{47}$$

- The *direction* of **q** must coincide with that of the RL vector $\boldsymbol{\tau}$. This condition can be achieved by rotating the crystal by an angle η around an axis perpendicular to the scattering plane (defined by $\mathbf{k}_i$ and $\boldsymbol{\tau}$).

- The crystal plane under consideration must coincide with the scattering plane — this is a condition on the χ angle of the detector (not shown).

We can interpret the three δ functions in eq. 39 as representing these three condition in their order. Observing further that for constant wavelength

$$\begin{aligned} \delta(q) &= \frac{\lambda}{2\pi\cos\theta}\delta(\gamma) \\ \delta(\bar{\alpha}) &= \delta(\frac{\gamma}{2}-\eta) = \frac{1}{2}\delta(\gamma-2\eta) \end{aligned} \tag{48}$$

we obtain

$$\begin{aligned} \frac{d\sigma}{d\Omega} &= N_c\frac{(2\pi)^3}{v_0}\frac{2\left[\frac{\lambda}{2\pi\cos\theta}\right]\left[\frac{1}{2}\delta(\gamma-2\eta)\right]\delta(\chi)}{q^2\cos\theta}\left|F(\boldsymbol{\tau})\right|^2 \\ &= N_c\frac{d^3}{v_0}\frac{2\sin\theta}{\cos^2\theta}\left|F(\boldsymbol{\tau})\right|^2\delta(\gamma)\delta(\gamma-2\eta) \end{aligned} \tag{49}$$

As before, we can integrate over the detector solid angle $d\Omega = \sin\gamma d\gamma d\chi$, by observing that

$$\int d\gamma\delta(\gamma)(\gamma-2\eta) = \delta(\eta) \tag{50}$$

leading to

$$\sigma(\eta) = N_c\frac{d^3}{v_0}2\tan\theta\sin\theta\left|F(\boldsymbol{\tau})\right|^2\delta(\eta) \tag{51}$$

Eq. 51 has the form we expect — there is no scattering unless the crystal is rotated to the $\eta = 0$ position. Let us imagine now to bathe the crystal in an incident beam with flux Φ and rotate it through the reflection position with angular velocity $\omega = d\eta/dt$. We want to determine how many particles are scattered in the process.

$$N_{scatt} = \Phi\int dt\sigma(\eta) = \frac{\Phi}{\omega}\int d\eta\sigma(\eta) = \frac{\Phi}{\omega}N_c\frac{d^3}{v_0}2\tan\theta\sin\theta\left|F(\boldsymbol{\tau})\right|^2 \tag{52}$$

Once again, eq. 52 can be corrected for absorption as for eq. 45.

Referring again to eq. 25, we can find the following expressions for the **Lorentz** factor $\mathcal{L}$ and the incident time-integrated flux $\mathcal{F}_{inc}$. Note that in this case **the integrated intensity does not depend on the total measuring time, but on the rotaton speed through the reflection**.

$$\begin{aligned} \mathcal{L} &= 2\tan\theta\sin\theta \\ \mathcal{F}_{inc} &= \frac{\Phi}{\omega} \end{aligned} \tag{53}$$

11.2 Integrated intensities from a random collection of small single crystals — powder diffraction

In this section, we will calculate the integrate cross section over he whole solid angle for a "random" collection of small single crystals (or crystallites) of the same material — in other words, a powder sample. We will make the slight simplification that all the crystallites have the same number of unit cells n_c.We can once again apply eq. 39 to obtain:

$$\frac{d\sigma}{d\Omega} = \frac{(2\pi)^3 n_c}{v_0} \sum_i \sum_{RL} \frac{\delta(\bar{q})\delta(\alpha - \alpha_i(\boldsymbol{\tau}))\delta(\chi - \chi_i(\boldsymbol{\tau}))}{q^2 \sin(\alpha)} \left|F(\boldsymbol{\tau})\right|^2 \tag{54}$$

Here, $\alpha_i(\boldsymbol{\tau})$ and $\chi_i(\boldsymbol{\tau})$ are the angular coordinates of RL vector $(\boldsymbol{\tau})$ for crystallite i. If the number of crystallites n_p is very large and their angular distribution is uniform ($n_c/4\pi$), we can replace the summation with an integral over the angular variables.

$$\begin{aligned} \frac{d\sigma}{d\Omega} &= \frac{(2\pi)^3 n_c n_p}{4\pi v_0} \sum_{RL} \int \sin\alpha(\boldsymbol{\tau}) d\alpha(\boldsymbol{\tau}) d\chi(\boldsymbol{\tau}) \frac{\delta(\bar{q})\delta(\alpha - \alpha_i(\boldsymbol{\tau}))\delta(\chi - \chi_i(\boldsymbol{\tau}))}{q^2 \sin(\alpha)} \left|F(\boldsymbol{\tau})\right|^2 \\ &= \frac{2\pi^2 N_c}{v_0} \sum_{RL} \frac{\delta(\bar{q})}{q^2} \left|F(\boldsymbol{\tau})\right|^2 \end{aligned} \tag{55}$$

where N_c is the number of unit cells in the *whole* powder sample. As for the previous examples with the single crystal geometries, we can focus on a *single* Bragg peak, but with the *caveat* that individual Bragg reflections cannot be completely isolated in powder diffraction. As shown in the Ewald construction of fig. 6, a uniform distribution of incident wavevectors with respect to the RL means that all RL nodes on the surface of a *sphere* will be in reflection conditions simultaneously. This means, at the very least, that all symmetry-equivalent RL nodes will scatter at the same time, a fact that is generally accounted for by introduce the **reflection multiplicity factor**, $m_{\boldsymbol{\tau}}$, so that

$$\frac{d\sigma}{d\Omega} = \frac{2\pi^2 N_c}{v_0} m_{\boldsymbol{\tau}} \frac{\delta(\bar{q})}{q^2} \left|F(\boldsymbol{\tau})\right|^2 \tag{56}$$

The Lorentz factors for the wavelength-dispersive and constant-wavelength geometries can now be easily calculated by introducing the appropriate transformations for $\delta(q)$.

11.2.1 Powder diffraction cross section — wavelength-dispersive case

We employ eq. 56 together with eq. 41 to obtain:

$$\frac{d\sigma}{d\Omega} = N_c \left(\frac{d^3}{v_0}\right) m_{\boldsymbol{\tau}} \left|F(\boldsymbol{\tau})\right|^2 \frac{1}{4\pi} \lambda\, \delta(\lambda) \tag{57}$$

whence, by accounting for the incident flux $\Phi(\lambda)$ and integrating over all wavelength and over the detector solid angle Ω_d we obtain the number of particles scattered into the detector per second:

$$P_{\boldsymbol{\tau}} = N_c \left(\frac{d^3}{v_0}\right) m_{\boldsymbol{\tau}} \left|F(\boldsymbol{\tau})\right|^2 \frac{\lambda\Phi(\lambda)}{4\pi} \Omega_d \tag{58}$$

Eq. 58 it is quite interesting: unlike the previous cases we encountered, the count rate on the detector is *proportional to the detector solid angle*. This is a reflection of the fact that, in this geometry, the Bragg reflection is observed at all scattering angles — of course each with different wavelengths.

Referring again to eq. 25, we can find the following expressions for the **Lorentz** factor $\mathcal{L}$ and the incident time-integrated flux $\mathcal{F}_{inc}$ (t is the measuring time).

$$\begin{aligned} \mathcal{L} &= \frac{\Omega_d}{4\pi} \\ \mathcal{F}_{inc} &= \lambda\Phi(\lambda)\, t \end{aligned} \tag{59}$$

11.2.2 Powder diffraction cross section — constant-wavelength case

We employ eq. 56 together with eq. 48 to obtain (the development is entirely similar:

$$\frac{d\sigma}{d\Omega} = N_c \left(\frac{d^3}{v_0}\right) m_{\boldsymbol{\tau}} \left|F(\boldsymbol{\tau})\right|^2 \frac{\tan\theta}{2\pi} \delta(\gamma) \tag{60}$$

Here, we assume that the detector has a large span in the scattering plane, encompassing the region where the Bragg peak occurs. Once again, we can integrate over the detector solid angle $d\Omega = sin(2\theta) d\gamma d\chi$ to yield:

$$P_{\boldsymbol{\tau}} = N_c \Phi \left(\frac{d^3}{v_0}\right) m_{\boldsymbol{\tau}} \left|F(\boldsymbol{\tau})\right|^2 \frac{\sin^2\theta}{\pi} \Delta\chi \tag{61}$$

where $\Delta\chi$ is the angular aperture of the detector along the Debye-Scherrer cones. For a typical diffractometer, the *height* of the detector out of the scattering plane, H, is constant, whereas the angular aperture of the detector along the Debye-Scherrer cones varies approximately as

$$\Delta\chi \simeq \frac{H}{R} \frac{1}{4\pi \sin\theta \cos\theta} \tag{62}$$

R being the radius of the diffractometer. The count rate is therefore

$$P_{\boldsymbol{\tau}} = N_c \Phi \left(\frac{d^3}{v_0}\right) m_{\boldsymbol{\tau}} \left|F(\boldsymbol{\tau})\right|^2 \frac{\tan\theta}{4\pi^2} \frac{H}{R} \tag{63}$$

Referring again to eq. 25, we can find the following expressions for the **Lorentz** factor $\mathcal{L}$ and the incident time-integrated flux $\mathcal{F}_{inc}$ (t is the measuring time).

$$\begin{aligned} \mathcal{L} &= \frac{\tan\theta}{4\pi^2} \frac{H}{R} \\ \mathcal{F}_{inc} &= \Phi\, t \end{aligned} \tag{64}$$

12 Bibliography

Stephen W. Lovesey, "Theory of neutron scattering from condensed matter" [1] is "the" textbook on the theory of neutron scattering and related matters. It is perhaps not always easy to find what one is looking for in this book...

G.L. Squires "Introduction to thermal neutron scattering" [2] is a classic introductory book on the subject.

E. H. Kisi "Applications of neutron powder diffraction" [3] is a more recent book on neutron diffraction, focussing on the powder method.

Warren, "X-ray diffraction" [4] is a rather old book with a very dated notation, but somehow I always find myself going back to it. Some of the explanations are very clear.

Authier, "Dynamical Theory of X-ray Diffraction" [6] is a very complete book on the dynamical theory of X-ray scattering. It has a good historical introduction and some simple explanations of the phenomena.

References

[1] Stephen W. Lovesey, “Theory of neutron scattering from condensed matter”, Oxford Science Publications, Clarendon Press, Oxford (1984) — in 2 volumes.

[2] G.L. Squires ”Introduction to thermal neutron scattering” Dover Publications, Cambridge, New York, 1978

[3] E. H. Kisi and C. J. Howard, ”Applications of neutron powder diffraction”, Oxford University Press, Oxford, New York, 2008.

[4] B.E. Warren, *X-ray diffraction* (Dover Publications, Inc., New York) 2nd Ed. 1990.

[5] G. Borrmann, Phys. Stat. Sol. (A) 204, No. 8, 2515 2527 (2007)

[6] André Authier, “Dynamical Theory of X-ray Diffraction”, International Union of Crystallography, Oxford University Press (Oxford, New York), 2001.